MEMS Electro Thermal Actuators: Modeling and Simulation

Submitted by:

Syed Muhammad Arslan Gilani 2015-MS-EE-29

Supervised by: Dr. Farooq Ahmad

Department of Electrical Engineering

University of Engineering and Technology Lahore

MEMS Electro Thermal Actuators: Modeling and Simulation

Submitted to the faculty of the Electrical Engineering Department
of the University of Engineering and Technology Lahore
in partial fulfillment of the requirements for the Degree of

Master of Science
in
Electrical Engineering

Submitted by:

Syed Muhammad Arslan Gilani 2015-MS-EE-29

Thesis Approved on October **29, 2018**

______________________	______________________
Dr. Farooq Ahmad (Internal Examiner)	Dr. Nauman Zafar Butt (External Examiner)

______________________	______________________
(Dr. K. M Hassan) For Chairman Department of Electrical Engineering	Dean Department of Electrical Engineering

Department of Electrical Engineering
University of Engineering & Technology Lahore
October-2018

Declaration

I **Syed Muhammad Arslan Gilani** S/O **Syed Muhammad Shafiq Ur Rahman Tahir Gilani**, Registration number **2015-MSEE-29**, Discipline Electrical Engineering candidate of **MS Electrical Engineering (Control Systems)** at the UET Lahore do hereby declare that research work titled **MEMS Electro Thermal Actuators: Modeling and Simulation** is submitted by me in partial fulfillment of MS Electrical Engineering, is my original work, and has not been submitted or published earlier. I also solemnly declare that it shall not, in future, be submitted by me for obtaining any other degree from this or any other university or institution.

It is further declared that I have developed this research work and the accompanied report entirely on the basis of my personal efforts made under the sincere guidance of my supervisor. The work has not been presented elsewhere for assessment. Where material has been used from other sources. It has been properly acknowledged/ referred.

Signed: ______________________

Date: ______________________

Acknowledgements

All praises and thanks to Al-Mighty "Allah", the most merciful, the most gracious, the source of knowledge and wisdom endowed to mankind, who conferred me with the power of mind and capability to complete this thesis to the exciting ocean of knowledge. All respects are for our most beloved Holy Prophet "Muhammad (SAW)", who is forever a torch of guidance for humanity as whole, and all the blessings that have been acknowledge below. Writing this thesis was a difficult task for me and I would like to say thanks to many people who helped and encouraged me to complete it. Without their help and support it would have been difficult for me to complete it.

First of all, I am thankful to my supervisor Dr. Farooq Ahmad for enabling me to complete my thesis. He gave me best guidance and encouraged me whenever I felt down. I am truly grateful to him for not losing patience with me when at times I fell short of his expectations.

I am also thankful to my fellow researchers who helped and encouraged me to complete this thesis in time and the lab staff to provide facilities for research work.

Finally, I would also like to thank my parents and siblings who supported at every moment of my educational career. Specially the one person who deserves my sincerest gratitude is my father, without him I would have been unable to complete my MS degree. His love, faith and belief in me had been a great inspiration for me.

Syed Muhammad Arslan Gilani
Lahore, October 2018

To my Parents and my slings, who always believed in me and were there for me at each and every stage of life.

Table of Contents

Acknowledgements iv
List of Figures viii
List of Tables ix
Abbreviations x
Abstract xi
Chapter 1. Introduction 1
1 Introduction 1
1.1 General Overview of MEMS Actuators: 1
1.2 Problem Statement: 3
1.3 Objectives: 3
1.4 Thesis Organization: 4
Chapter 2. Literature Review 5
2 Literature Review: 5
2.1 Background of Electro-Thermal Actuator (ETA): 5
2.2 Types of Electro-Thermal (ET) Actuators: 7
2.2.1 U-Shaped ET Actuators: 8
2.2.2 V-Shaped ET Actuators: 9
2.2.3 Z-Shaped ET Actuator: 9
2.2.4 H-Shaped ET Actuator: 10
Chapter 3. Design and Micro-Fabrication 12
3 Design and Micro-Fabrication 12
3.1 Design of MEMS Electro Thermal Actuator 12
3.2 Device Design Parameters 13
3.3 Electro-Thermal Actuation 15
3.3.1 Actuation principle 16
3.4 Mechanical Modeling of Device 17
3.4.1 Output Amplitude 18
3.4.2 Maximum Differential Amplitude: 18
3.4.3 Damping Ratio: 19
3.4.4 Quality Factor: 19
3.4.5 Device Damping: 19
3.4.6 Resonance Frequency: 21

3.5 Temperature of Device 21
3.6 Virtual Fabrication: 22
3.6.1 Blueprint: 22
3.6.2 Intelli Fab: 24
3.6.3 Fab sim 26
3.6.4 TEM Module 29
Chapter 4. Results and Discussions 31
4 Results and Discussions 31
4.1 Results: 31
4.1.1 Connectivity Test: 31
4.1.2 Uniformity in Layers: 31
4.1.3 Power Consumption: 32
4.1.4 Heat Flux 33
4.1.5 Rise in Temperature: 33
4.1.6 Change in Displacement 34
4.1.7 Thermal Actuation Force: 35
4.1.8 Amplitude Vs Driving Frequency: 36
Chapter 5. Conclusion and Future Work 38
5 Conclusion and Future Work: 38
5.1 Conclusions: 38
5.2 Future Work: 38
5.2.1 Actuator: 39
5.2.2 Micro Flying Robot: 39
Appendix I 40
Appendix II 43
Reference 56

List of Figures

Fig 1: U-Shaped ET Actuator. (a) USA with Series Wiring (b) USA with Parallel Wiring ..8
Fig 2: V-Shaped ET Actuator (VSA), (a) Buckle-Beam VSA , (b) Shuttle based VSA 9
Fig 3: Z-Shaped ETA (ZSA)..10
Fig 4: H-Shaped ETA(HSA)...11
Fig 5: Proposed design of ETA based micro flying robot 13
Fig 6: (a) Bimetallic cantilever beam in normal position (b) Bimetallic bending ($\alpha_1 < \alpha_2$) .16
Fig 7: Geometry of bent beam 17
Fig 8: (a) Mask of wing attached with static part (b) Mask of wiring and connection pads 23
Fig 9: (a) Overall masks for the virtual fabrication (b) Legend...23
Fig 10: Layers by layer device designing using masks for different layers..........................24
Fig 11: (a) Polysilicon deposited layer (b) polysilicon resistor 25
Fig 12: (a) Creation VIA and deposition of tungsten in it (b) creation of aluminum first layer 25
Fig 13: (a) Exposure for cutting of Si (b) Silicon etched (c) All unnecessary material etched to free Wing 26
Fig 14. Cross sectional view of virtual fabrication in fab sim 27
Fig 15 Micro flying robot chip based on CMOS-MEMS ETA 28
Fig 16: All above results are simulated in TEM module at 1V 30
Fig 17: Input Voltages Vs Current in ETA beams...32
Fig 18: Applied Voltage Vs Electric Field 32
Fig 19: Input Voltages Vs Power Density 33
Fig 20: Input Voltages Vs Heat flux..34
Fig 21: Applied Voltage Vs Change in Temperature 34
Fig 22: Input Voltage Vs Change in displacement at proof mass tip 35
Fig 23: Applied Voltage Vs Thermal Actuation Force..36
Fig 24: Amplitude Vs Driving Frequency in Dynamic Mode 36

List of Tables

Table 1: Optimized directions of electro-thermal actuator (ETA)..13
Table 2: Design parameters of MEMS ETA for flying micro robot.....................................14
Table 3: Properties of materials used in MEMS ETA 14
Table 4: ETA contact pad description 28

Abbreviations

MEMS	Micro-electro-mechanical System
CMOS	Complementary Metal Oxide Semiconductor
IC	Integrated Circuit
ETA	Electro-thermal Actuator
USA	U-Shaped Actuator
VSA	V-Shaped Actuator
ZSA	Z-Shaped Actuator
HSA	H-Shaped Actuator
PZR	Piezo resistor
LPCVD	Low Pressure Chemical Vapor Deposition
RIE	Reactive Ion Etching
DRIE	Deep Reactive Ion Etching
Metal MUMP	Metal Multi User MEMS Process
Poly MUMP	Poly Multi User MEMS Process
SOI-MUMP	Silicon On Insulator Multi User MEMS Process
VOA	Variable Optical Attenuator
TCR	Temperature Coefficient of Resistance
CTE	Coefficient Thermal Expansion
FEA	Finite Element Analysis
TEM	Thermo-Electro-Mechanical

Abstract

In recent years, MEMS sensors and actuators are getting more attention in daily life application due to its compactness, miniaturization, inexpensive and highly efficient as compare to the other ordinary devices. In this research work ETA is modeled and simulated. Complementary Metal Oxide Semiconductor (CMOS) MEMS technology is used to design, fabricate and characterize ETA using MATLAB and INTELLISUITE software. Micro actuator is used in the wing of micro flying robot and it consist of four supporting beams. For upward movement of micro flying robot, wing is resonated in its first mode of vibration. Beam is made up of polysilicon and aluminum using bimorph actuation mechanism where polysilicon works as heating resistor. In dynamic mode the maximum amplitude of device is 124.15mm with the quality factor of 107.78 at the resonance frequency of 843Hz mathematically. While in simulation maximum amplitude of 97.82mm is obtained with the quality factor of 105.38 at the resonance frequency of 970Hz. The actuation force to drive the cantilever in dynamic mode is 3.26μN mathematically and 4.67μN in simulation. In static mode at 2V the mathematical and simulated results are approximately same, 28.6mW power is used at 2V for the displacement of 129μm.

Chapter 1

Introduction

1.1 MEMS Actuators:

Advancement in the field of science and technology is dependent on different sensing and actuations process to perform any action and change in the system. These sensing and actuating mechanisms brings considerable changes in the systems such as biomedical field, telecommunication, satellite communication, Optical communication, automation in industrial process, navigation systems, safety and health field, aircrafts, aerodynamics and agriculture field etc. These sensing and actuation mechanism also done with existing technology on the basis of different principles, but the old technologies required high power for actuation process, large footprint, and high cost with meaningless performance and sensitivity[1].

The Micro Electro Mechanical System (MEMS) is a most general form of technology, which can be well-defined as miniaturized mechanical structures and electro-mechanical elements (like structures assembly and devices), made by using different microfabrication techniques. MEMS are distributed in four major portions Microelectronics, Micro structures, Micro sensors and Micro actuators. Where microelectronics plays the role of brain for controlling mechanism of micro structures, sensors are responsible of detection/ sensing the change in the system e.g. force, biomedical, chemical, IR sensors etc. and actuators are used for the controlling mechanism effectively and efficiently used in micro pumps, micro grippers, optical switches etc. The MEMS devices facilitate the user such as availability at low cost with reduced size at low power consumption and need few voltages to operate etc. [2]

In the development of MEMS, micro actuators are very important part which are used for driving mechanism. Broadly speaking, actuation at micron level is energy transduction processes and produce some action. In other words, actuators in MEMS are the devices which are used to produce force or displacement via some suitable method to transform electrical energy to mechanical energy[3]. Actuators are used in micro grippers[4][5], micro mirrors[6][7], micro pumps[8], micro switches[9], and

optical switches etc. In actuators, micro-cantilever is a basic structure and tip deflection at the other end is used for actuation purpose. There are several methods to actuate the actuators like piezoelectric, electro-magnetic, electrostatic and electro-thermal actuators.

In piezoelectric actuation electric field is used to generate strain in the material which produces actuation in the form of displacement and force. It provides high output force and large switching speed at low input driving voltages. In Electromagnetic actuation some special kind of material required to use in micro fabrication to actuate device electromagnetically when input current is applied. It provides high output force, fast switching speed, low power of operation at few input driving voltages. Its fabrication is not so simple as compared to electrostatic and electro-thermal (ET) actuator. In electrostatic actuators electrostatic force generated between two electrodes when potential is applied at input side. Electrostatic force attracts the one moveable plate towards the fixed one and provides displacement. They provide small output force and displacement at high driving voltages[9]. The electro-thermal actuation (ETA) is one of the most important mechanism for actuation. Its provides high output force and displacement at low operating/driving voltages. When potential is applied electric current passes through the material and produces heat due to resistance of material which rises temperature. Thermal expansion occurs in the material due to rise in temperature according to the joule heating principle[10].

There are two main categories of electro-thermal actuation according to the direction of motion. One is in-plane actuation[11] and other is out-of-plane actuation[12]. In-plane electro-thermal actuators(ETA) are fabricated using surface micromachining while out-of-plane electro-thermal actuators(ETA) fabricated using bulk micromachining. Bulk micromachining process is complex then surface micromachining but its more effective for out-of-plane actuation and usually used in out-of-plane actuators instead of use in in-plane actuators. Currently five types of electro-thermal actuators are used depends on shape, which includes Bi-Morph cantilever[13], U-shaped[14], V-shaped[15], Z-shaped[16] and H-shaped[17]. These are briefly discussed in chapter 2. All these actuators work on joule heating effect principle. These ET actuators are fabricated using various technology such as metal-MUMPs, poly-MUMPs, SOI-MUMPs and CMOS etc.

CMOS is the abbreviation of complementary metal oxide semiconductor. It is one of the most important technology for MEMS device fabrication in modern research. CMOS is technology used in integrated circuits (IC) and also used commercially for MEMS ETA fabrication. The main advantage of CMOS technology is its low power consumption, smaller size, reduction in cost, improved performance and high immunity to noise. [18] CMOS compatible approach with MEMS devices allows higher performance with small size of device. Top layer is used to protect entirely the CMOS circuitry which layer is used as mask layer to define MEMS structure during post micromachining process. The integration of CMOS technology with MEMS technology is known as CMOS-MEMS technology. Therefore this process is known as CMOS compatible process.[19]

1.2 Problem Statement:

MEMS ETA are used in different industrial and biomedical equipment's. Conventional ETA uses large power(>100mW).

- H-Shape ETA require high voltages for operation (up to 22V). H, V and Z-shape has high output force and reasonable displacement but have high mechanical stiffness which limits their actuation bi-directionally and increase the required input voltages.
- The study of “Development of Miniature Camera Module Integrated With Solid Tunable Lens Driven by MEMS-Thermal Actuator” shows lesser displacement(135um) even at relatively high voltages (10V).
- Recent research where “Thermal Reliability of ETA MEMS Mirror” was studied shows tungsten interconnects burnt due to rise in temperature.

1.3 Objectives:

The main objectives of this research project are

- To design and optimize high displacement, low driving voltage Electro Thermal Actuator (ETA) on CMOS-MEMS chip.
- To mathematically model ETA using MATLAB in terms of power consumption, max displacement, temperature and force.
- To characterize the optimized ETA performance in simulation environment.

1.4 Thesis Organization:

In this research work CMOS MEMS based electro-thermal actuator is proposed which will be used in micro flying robot. The thesis organization is given below:

Chapter-1:

General overview and the objectives of the research work are covered in this chapter.

Chapter-2:

This chapter covers the background of the actuators, actuating mechanisms, Types of actuators as well as the benefits of different types of actuators. This chapter also justify the reason of using bimetallic actuator strip.

Chapter-3:

In this chapter, mathematical modeling, design and simulation of CMOS based electro thermal actuator is discussed. The working principle of the thermal actuator is explained. The types and the properties of materials required for the development of actuator are also discussed. At the end of this chapter, the actuator is virtually fabricated in intellisuite software environment.

Chapter-4:

This chapter describes the simulation results which are compared to the theoretical results and discussed.

Chapter-5:

The conclusion and future directions of this research work is described in this chapter.

Chapter 2

Literature Review:

2.1 Background of Electro-Thermal Actuator (ETA):

Actuator is a component which is responsible for the controlling mechanism. In Micro Electro Mechanical systems (MEMS), micro actuators are the devices which are used to produce force and displacement by transducing an input given in electrical domain to the output in mechanical domain. These changes have intermediate energy domains either directly or indirectly. MEMS actuators are used to convert energy into some proper action which is accomplish for generating some motion in micro scale for individual elements positioning.

MEMS micro actuators are divided into four different groups according to their working/actuation mechanism. Piezoelectric, electro-magnetic, electro-static and electro-thermal micro actuator are these four main classes[3]. Special kind of material is required for the micro fabrication process of piezoelectric and electromagnetic actuators. Electrostatic actuators give small controllable range of displacement with less functional robustness. Electro-thermal actuator (ETA) provides large output force, stable and controllable displacement (amplitude). Thermal actuation in micro scale devices has been demonstrated as a compact, high-force actuation technique which compliments electrostatic actuation. Joule heating is typically used to power these actuators, which generally operate at lower and more desirable voltages than electrostatic devices[20]. ETA have standard Integrated circuit (IC) micro-fabrication process compatibility as well as material. Among the other actuators, MEMS thermal actuators usually used polycrystalline silicon material either heat generating source in metal based thermal actuators or to fabricate the thermal actuators which are poly silicon based[21]. In some cases, as the temperature profile of thermal actuator changes, the poly silicon resistivity also changes. Therefore, it is essential for poly-silicon resistivity characterization to realize the ET actuator behavior or to improve more precise model[22].

Judy et al. introduced the first in-place MEMS electro thermal micro actuator using high resistance poly silicon beams which encompassing serpentine micro bridge and alternately coated with platinum. “Hot-arm” actuator, “heatuator”, “pseudobimorh” or “U-shaped” actuator topology demonstrated by Guckel et al. which was fabricated using a sacrificial LIGA (lithographie- galvanoformung- abformung) process in nickel. The actuators which fabricated by poly silicon with double hot-arms topology to enhanced the efficiency of the actuator was described by Comtois et al. in which the temperature difference was increased between cold and hot-arm by the removal of cold-arm from electrical current path. “V-shaped”, “chevron,” or “bent-been” Electro thermal actuator topology first demonstrated by Noworolski et al. This topology was originated for the sensor which use as passive strain by Najafi and Gianchandani et al. Recently, Single and cascaded bent-beam actuators topology also reported by Que Et al. Thermal expansion principle based U-shaped electro thermal poly silicon actuator with thin or thick arm developed by Tichem, Henneken and Sarro et al. Thermal expansion based principle micro cantilever ETA consist of single material. Differential of thermal expansion principle in only applied for multilayer ETA. Multilayer ETA (two layer ETA)with thickness of optimum layer was reported by Hsu, Cheng, Lai and Chan et al. Electro thermal analytical three layer micro actuator modeling was investigated by Hilleringmann, shui and Jiang et al. Downward and upward bending of bi-material was reported by Hsu, Huang, Chung and Cheng et al[3].

The actuators which are widely used in MEMS actuation mechanism, are electrostatic and electro thermal actuators. These two classes of actuators have very different characteristics although these actuators have same basic electrical energy utilizing functions to produce output force and displacement. The electrostatic based micro actuators have typically small deflections either require high driving voltage for large deflections or dimensional tolerances closed. These actuators are usually more desirable because they operate at high frequency and low output power[23]. On other end, actuators which are based on thermal expansion have advantage of large driving output force and large displacement with very low driving voltage. The electro thermal micro actuators provides large perpendicular or parallel deflections to the substrate output force[24].

As we compared to the electrostatic micro actuators, electro-thermal (ET) actuators are less efficient in quick actions and limited in some applications like micro

biological samples handling. Actually the dynamic design of this actuator is the main cause behind this deficiency. In previous research of this ET actuator, U-shaped ET actuator mechanical modeling addressed which dynamically designed. The behavior of U-shaped ET actuator was dynamic and the response of thermal mechanical modeling was as quasi-static. There is no accurate analysis and analytical modeling has been described in which the dynamically response addressed of V-shaped and Z-shaped ET actuators according to the authors[25]. Therefore, static level leads to accuracy in design of dimension parameters and the behavior of V-shaped and Z-Shaped ET actuator. Micro actuators fall into two different types which are in-plane and out-of-plane according to different motion forms. Further, all these ET actuators works on the basis of joule heating effect principle of material thermal expansion.

My research in this thesis work is to design and model ETA using bimorph cantilever beam for movements of wings of the micro flying robot. Bimorph cantilever beam ETA is basic type of actuator whose fabrication, design and implementation is easy as compared to other electro thermal actuators. The cantilever beams are made of aluminum and polysilicon with alternatively used silicon dioxide among each layer in structure. CMOS technology is used for the fabrication of this actuator.

2.2 Types of Electro-Thermal (ET) Actuators:

There are many types ET actuators but the U-shaped, V-shaped, Z-shaped and H-shaped ET actuators are basic types which are described as follows. The CMOS-MEMS bimorph cantilever beam is discussed in detail in chapter 3. Bimorph actuators have many advantages of large scan angle, low voltage for operation and high fil factor. But still its reliability issues still not properly understand[26].

2.2.1 U-Shaped ET Actuators:

U-Shaped actuator (USA) is also known as pseudo bi-morph actuator. Pseudo bi-morph actuator consist of cold and hot arms associated with anchors. same material is used in narrow and wide arm of the actuator. Therefore, the thermal expansion coefficient (TEC) of the actuator is also same. Hence the temperature difference generated in the hot and cold arm which is the main reason to actuate the U-shaped ET actuator. Because the hot arm of the USA is thinner than the cold arm, more current resistance exists in the hot arm. The more heat is generated which leads to some extension in the hot arm. Therefore, displacement is produced due to the thermal expansion of the hot arm. As a result, USA bends towards the cold arm. Therefore, this displacement is circular as an arc shape. U-shaped ET actuator can produce displacement on both directions i.e. either towards cold arm or towards hot arm. When you require to move it towards cold arm, you need to apply voltage difference in series configuration of the anchors. But when you require to move is towards hot arm, you need to apply voltage difference in parallel configuration of the anchors as shown in fig.1. Therefore, USA is usually used for bi-direction displacement purposes[27].

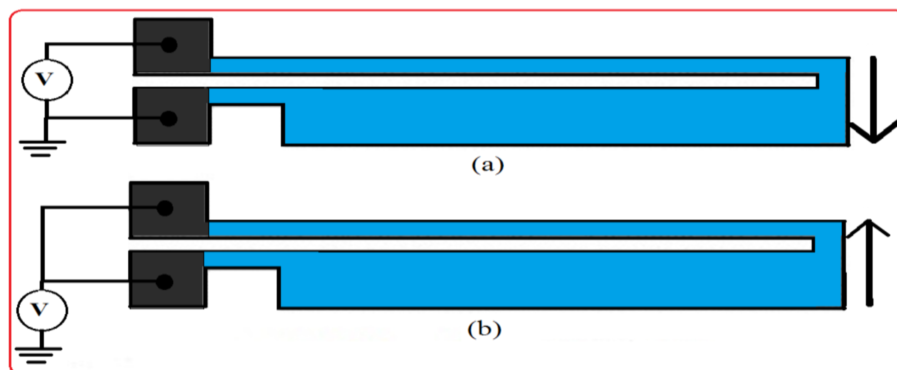

Fig 1: U-Shaped ET Actuator. (a) USA with Series Wiring (b) USA with Parallel Wiring

These typical actuators require small footprint size and used for micro-gripping, micro-position, manipulations and many other micro-scale and Nano-scale applications. The typical order of lateral displacement of USA is some μm. The lateral displacement is typically proportional to the thermal expansion of the material. The small deflection is generally equal to thermal expansion of the material multiplied by the length of the actuator and divided by separation of cold and hot arms[28].

2.2.2 V-Shaped ET Actuators:

V-shaped actuator (VSA) is also known as chevron electro-thermal (ET) actuator. Chevron ET actuator consist of two hot beams (hot arms) connected with anchors at free end where the voltage is applied. These two hot beams either directly connected to each other with small angle θ or connected to central shuttle and known as chevron or V-shaped ET actuator. The central shuttle has polysilicon resistance in it. The directly connected hot beams structure is also known as buckle-beam actuator as shown in fig.2.2 (a). A typical shuttle based V-shaped ET actuator is shown in fig.2.2 (b). VSA is usually fabricated by bimorph polysilicon and silicon dioxide material using post-CMOS micromachining technology. when the voltage is applied to the anchors of the VSA, current pass through hot beams. Therefore, high temperature is generated due to high current density in both narrow beams. These narrow hot beams extend in its length due to production of high temperature. The compatible voltage and current with standard IC (CMOS) are applied to operate the actuator by the polysilicon resistivity. As a result, some motion is produce in central shuttle this produced displacement is due to the this thermal expansion in the actuator[28].

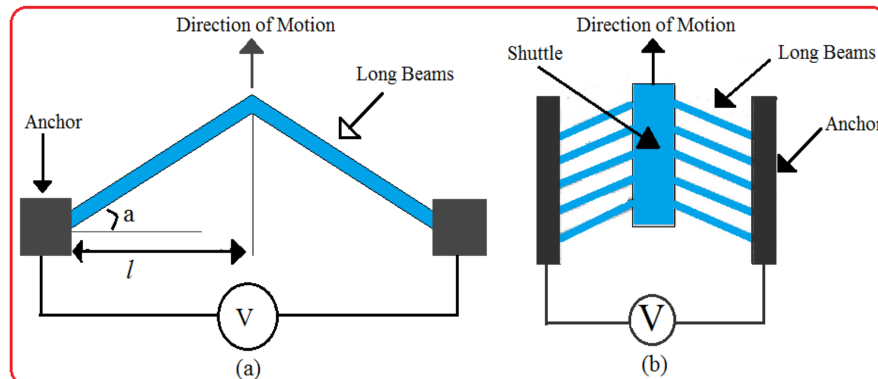

Fig 2: V-Shaped ET Actuator (VSA), (a) Buckle-Beam VSA , (b) Shuttle based VSA

2.2.3 Z-Shaped ET Actuator:

Z-shaped Actuator (ZSA) is similar in structure to the V-shaped actuator (VSA) but there is small difference in the beams of the both actuators[25]. The narrow beams (hot arms) are symmetric to Z shape. The both Z shape beams are connected to the anchors of the actuator at the free end but these two beams are connected to the central shuttle. The Z shape beams are further divided into long beams (denoted by L) which

is horizontal part of the beams and short beams (denoted by l) which is vertical part of the beams[16]. The Typical Z-shaped actuator (ZSA) is shown in fig. 2.3.

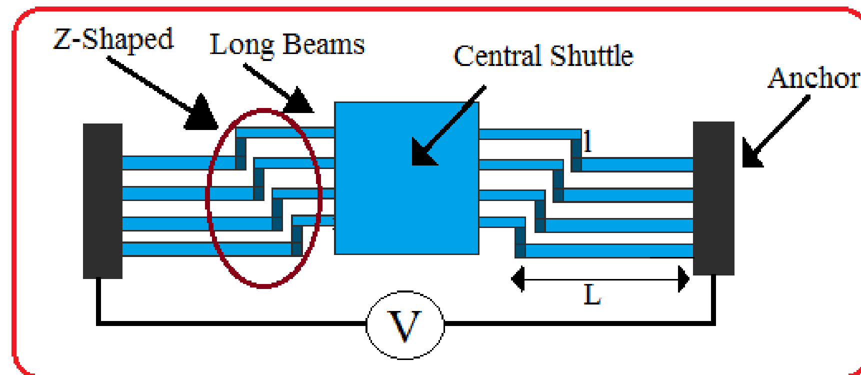

Fig 3: Z-Shaped ETA (ZSA)

The central shuttle has bimorph polysilicon resistance in it. ZSA is usually fabricated by bimorph polysilicon and silicon dioxide material using post-CMOS micromachining technology. The metal inter-connect to the dielectric inter-layer and CMOS foundry silicon substrate in post-CMOS micromachining technology. When the voltage is applied to the anchors of the ZSA, high temperature is generated due to high current density in both narrow Z shape beams according to joule heating effect. These hot arm or Z shape beams extend in its length due to production of high temperature especially in long beams (whose length denoted by L). Due to symmetry in the beams length, long beams (L) do not extend. The extension of long beams length accommodates to the short beams (whose length denoted by l) which is vertical part of the beams. This is the thermal expansion of the beam due high temperature inducement. As a result central shuttle motion is achieved due to net elongation of the Z shape beams[29]. Therefore, rectilinear displacement is achieved by this type of actuator as similar to V-shape thermal actuator.

2.2.4 H-Shaped ET Actuator:

H-shaped actuator (HSA) consists of two long beams, four anchors and one link beam. Each long beams are connected with two anchors on both sides of the beams and the link beam is connected to middle position of two long beams to make H shape. Therefore, these four anchors which are used as electrical pads, are located on the four corners of the actuator. A typical H-shape actuator is shown in fig.2.4.

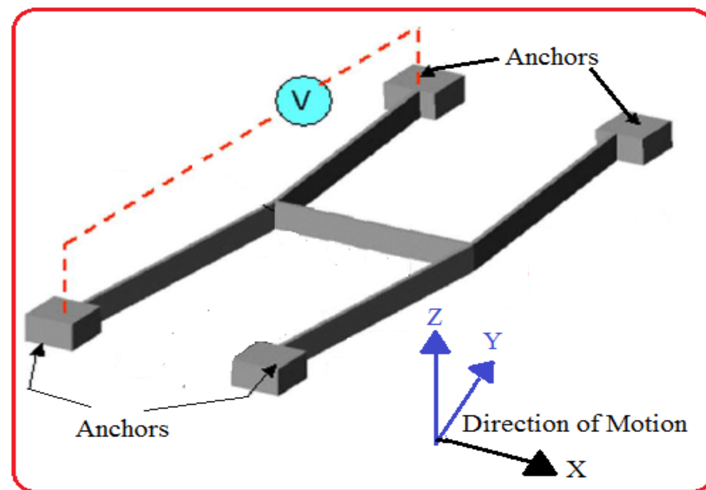

Fig 4: H-Shaped ETA(HSA)

Each anchor is made by silicon Si material and beams are made by bimorph polysilicon and silicon dioxide materials which are fabricated by post-CMOS micromachining technology. The compatible voltage and current with standard IC (CMOS) are applied to operate the actuator by the polysilicon resistivity. We apply the DC voltage to the both anchors of the HSA beam, current pass through the long beams. High temperature produces due to high current density in long beams according to joule heating effect principle. Therefore, some extension produces in the long beams of the actuator due to the thermal expansion in the material and move the beams towards right direction. This direction of motion and the net displacement depends on the applied voltages. We can obtain the larger displacement by this type of actuator. The anchors and beams of the HSA have high aspect ratio[30].

Chapter 3

Design and Micro-Fabrication

3.1 Design of MEMS Electro Thermal Actuator

MEMS electro-thermal actuator based on bi-metallic cantilever using bimorph structure are given more attention for their use in robotics which will tiny in size, having low cost and required less operating power. There are number of techniques used for the actuation purpose but electro-thermal actuation is commonly used for actuation in MEMS devices because its micro-fabrication process is easy and it also provide CMOS compatibility for integrated circuits (IC). The actuator is designed for the purpose of movement of wings in the micro flying robot. This CMOS-MEMS actuator have not only the advantage of small size, low cost, minimum power consumption but it also provides large actuating force.

The structure is CMOS based so we are bound to use the materials which can be used in CMOS technology. In CMOS we have the limit of using elements which contain Silicon (Si), Silicon di Oxide (SiO_2), Poly Silicon, Aluminum (Al) and Tungsten (W). The structure contains Silicon as base structure (Si), Silicon di Oxide (SiO_2) as insulation between each layer, high-res poly silicon, and low-res poly silicon as resistor/heater, aluminum (Al) is for electrical wiring and actuating beam and tungsten (W) is for the VIAs for connections between two layers. Four cantilever beams are designed on both sides of the structure which are connected with the proof mass at their end. In the structure voltages are applied to draw current through the cantilever beams for the purpose of electro-thermal actuation of wings.

3.2 Device Design Parameters

The dimensions of the CMOS MEMS based electro-thermal actuators of micro flying robot are optimized to a certain value where it can provide more displacement, at low input voltages from one volt to five volts (1V ~ 5V), having low power consumption from mili watts to micro watts (mW to µW), having small mass in micro to Nano grams to minimize friction of air and damping. MATLAB and intellisuite software are used for the modeling, designing and optimization of cantilever beam ETA which provides an integrated environment for the designing of MEMS device. Proposed structure of cantilever beam is show in fig.5. where orange part is static part and blue part in moveable part and work as wing.

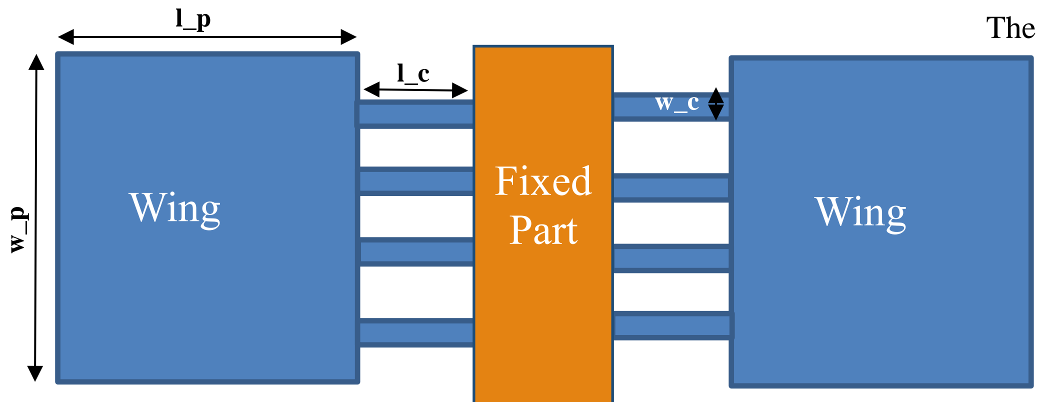

Fig 5: Proposed design of ETA based micro flying robot

Optimized parameters of the cantilever beam ETA are given in table 1. Detailed designed parameters are shown in table 2. Some of the material properties which are used in the structure are given in table 3.

Sr.#	**Symbols**	**Parameters**	**Value (µm)**
01	*l_c*	Cantilever beam length	200
02	*w_c*	Cantilever beam width	40
03	*t_c*	Cantilever beam thickness	1.224
04	*l_p*	Proof mass length	700
05	*w_p*	Proof mass width	700
06	*t_p*	Proof mass thickness	1.224

Table 1: Optimized directions of electro-thermal actuator (ETA)

Sr.#	Symbols	Parameters	Value (μm)
01	l_3	Polysilicon Beam length	200
02	l_4	Aluminum Beam length	200
03	l_5	Tungsten Beam length	1.074
04	w_3	Polysilicon Beam width	40
05	w_4	Aluminum Beam width	40
06	w_5	Tungsten Beam width	10
07	t_1	Silicon thickness in structure	50
08	t_1	SiO2 thickness in structure	0.3
09	t_3	Polysilicon Beam thickness	0.3
10	t_4	Aluminum Beam thickness	0.624
11	t_5	Tungsten Beam thickness	20
12	p_l	Contact pad length	200
13	p_w	Contact pad width	200
14	l_p	Proof mass length	700
15	w_p	Proof mass width	700
16	t_p	Proof mass thickness	3.372
17	t_T	Total Thickness of structure	53.372

Table 2: Design parameters of MEMS ETA for flying micro robot

Material	Symbol	Properties	Value	Unit
Silicon	*Si*	Young's Modulus	190	GPa
		Density	2328	Kg/m3
		Thermal Expansion Coefficient	3.20E-06	1/K
Silicon di Oxide	SiO_2	Young's Modulus	160	GPa
		Density	2300	Kg/m3
		Thermal Expansion Coefficient	2.90E-06	1/K
Poly Silicon	*H-Poly*	Young's Modulus	169	GPa
		Density	2300	Kg/m3
		Thermal Expansion Coefficient	2.91E-06	1/K
Aluminum	*Al*	Young's Modulus	70	GPa
		Density	2700	Kg/m3
		Thermal Expansion Coefficient	2.30E-05	1/K
Tungsten	*W*	Young's Modulus	41	GPa
		Density	19250	Kg/m3
		Thermal Expansion Coefficient	45E-07	1/K

Table 3: Properties of materials used in MEMS ETA

3.3 Electro-Thermal Actuation

Actuation in microscale devices and assemblies can be obtained by inserting or removing heat. Changes in temperature profile is result in mechanical displacement or force output, through thermal expansion[31]. Electro thermal is the phenomenon in the material that when current passes through the material, due to the movement of material molecules it faces difficulty to pass through and collides with the material particles, due to the collisions of particles heat is generated, which is known as heat loss in power systems. This resistance is directly proportional to the length of the material and its resistivity and inversely proportional to the area of the material. In case of a wire area is the product of width and thickness. There are three possible ways of transfer heat from one point to another.

1. **Thermal conduction** is the heat transfer in solids while temperature gradient is present.
2. **Thermal Convection** is the heat transfer from one surface to a stationary body of fluid.
3. **Thermal Convection** is the heat loss or gain during electromagnetic radiation propagation in air or vacuum.

$$R = \rho \frac{l}{A} \tag{3.1}$$

Where l, A and ρ are the length, cross sectional area and resistivity of the aluminum material. The value of resistivity of aluminum material is $2.82 \times 10^{-8} \Omega m$. The relationship between the resistance and the temperature is given in form of resistance as a function of temperature (at low temperature from 0 to 600°C) which can be expressed by equation 3.2.

$$R(t) = R_o\{1 + \alpha(t - t_o)\} \tag{3.2}$$

Where α temperature coefficient of resistance (TCR), R is the resistance of the temperature sensor (PZR) at t temperature and R_o is the resistance at ambient temperature t_o.

3.3.1 Actuation principle

The ETA using thermal bimorph consists two materials which are bounded along their longitudinal axis and acting as a single mechanical element. A thermal bimetallic actuator may contain more than two layers of materials such as for three layers of material structure is known as tri-morph bimetallic stip. Below figure shows a cantilever beam containing two layers, made with material 1 and material 2, both materials having same length and width but the coefficient of thermal expansion (CTE) of both materials is different. The subscript shows the material layer. Similarly, the width, thickness and young's modulus are represented. When temperature rises uniformly length of two materials changes unequally. As the two-layers of materials are joined tightly at the boundary, the beam start curving towards the material layer having lower CTE value. The diagonal bending is produced.

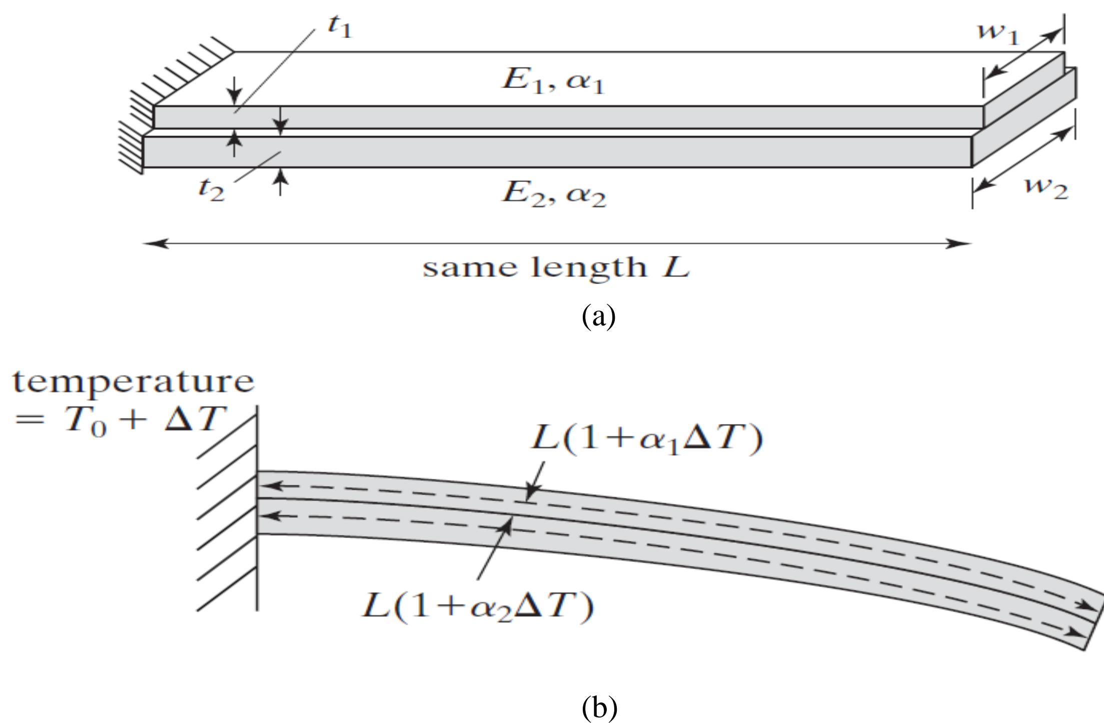

Fig 6: (a) Bimetallic cantilever beam in normal position (b) Bimetallic bending ($\alpha_1 < \alpha_2$)

Under a uniform change in temperature ΔT the beam shows bending and makes a curve it looks the shape of the section of an arc having length of arc is L. The radius of curvature of arc is calculated using equation 3.3.

$$\frac{1}{r} = \frac{6w_1w_2E_1E_2t_1t_2(t_1+t_2)(\alpha_1-\alpha_2)\Delta T}{(w_1E_1t_1^2)^2+(w_2E_2t_2^2)^2+2w_1w_2E_1E_2t_1t_2(2t_1^2+3t_1t_2+2t_1^2)} \quad (3.3)$$

The arc is section of the circle with a radius of curvature shown as r, covering the arc angle θ. The value can be determined by

$$\theta = \frac{l}{r} \quad (3.4)$$

Now we get the radius of arc and the angle by using these values now we are able to use trigonometry for the calculation of displacement in vertical direction as shown in fig.8. The verticle diplacement of free-end cantiliver beam is given by the equation 3.5.

$$d = r - r\cos(\theta) \quad (3.5)$$

3.4 Mechanical Modeling of Device

The mechanical behavior of the oscillating beams of the device under the electro thermal force is given by mass spring system where

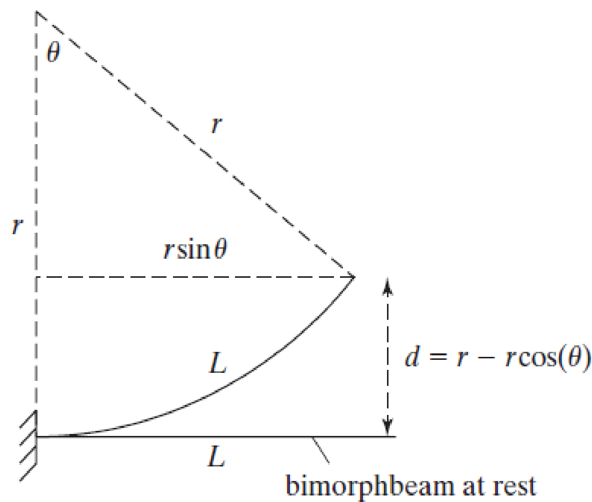

Fig 7: Geometry of bent beam

$$k_b = \frac{EW_bH_b{}^3}{4L_b{}^3} \tag{3.6}$$

$$m_b = V_b\rho_{avg} \tag{3.7}$$

Where k_b is spring/stiffness coefficient, E is young's modulus, m_b is the mass of cantilever beam, V_b is volume of cantilever beam and p_{avg} is the average volume of the materials used in cantilever beam which are silicon di oxide, aluminum and polysilicon.

3.4.1 Output Amplitude

The output amplitude or displacement of a device is calculated theoretically using steady state solution. We determined the output amplitude theoretically of flying robot device under the ET actuation by the equations detail in Appendix I. Thus the output amplitude (∇A) is calculated by

$$\nabla A = \frac{\left(\frac{Etw^3d_l}{4l^3}\right)\Big/m_b}{\sqrt{(\omega_o^2 - \omega_d^2)^2 + (\gamma\omega_d)^2}} \tag{3.8}$$

Where m_b is mass of beam under thermal actuation force, ω_o, ω_d and γ are the natural frequency, driving frequency of the wing and the damping constant. The relation among the damping ratio (ξ) and natural frequency (ω_o) is given by equation 3.9.

$$\gamma = 2\xi\omega_o = \frac{b}{m} \tag{3.9}$$

3.4.2 Maximum Differential Amplitude:

When the driving frequency (ω_d) is increased in such a way that driving frequency (ω_d) become equal to natural frequency (ω_o), then the resonance occurs. The frequency at this stage is known as resonance frequency. When the resonance frequency occurs, the maximum differential amplitude (∇A_{max}) is obtained. The maximum differential amplitude (∇A_{max}) is given by equation 3.10 as:

$$\nabla A_{max} = \frac{\left(\frac{Etw^3d_l}{4l^3}\right)}{m\omega_o\gamma} \tag{3.10}$$

3.4.3 Damping Ratio:

The damping ratio of the resonating shuttle based MEMS actuator is defined as the ratio of damping constant to the double of natural frequency of the resonating device. In other words, damping ratio is also defined as the ratio of actual damping coefficient to the critical damping coefficient of the resonating device. Thus theoretically, the damping ratio is calculated by the equation 3.11.

$$\xi = \frac{\gamma}{2\omega_o} = \frac{1}{2Q} = \frac{b}{2m\omega_o} = \frac{b}{b_c} \tag{3.11}$$

Where $b_c = 2\sqrt{km}$, Q is the quality factor b is the actual damping and b_c is the critical damping.

3.4.4 Quality Factor:

The quality factor (Q) is one of the important parameter which tell about the performance of the resonating actuator device. It can be determined from the behavior of the resonance. Further, the ratio of the energy stored to the energy loss per cycle in the system is also called quality factor (Q). Actually, the quality factor of the device describes response of the resonating MEMS device at specific frequencies. Mathematically, the quality factor of the electro thermally actuated MEMS resonator is determined by the equation 3.12.

$$Q = \frac{\omega_o}{\gamma} = \frac{f_r}{\Delta f_{3dB}} = \frac{m\omega_o}{b} = \frac{1}{2\xi} \tag{3.12}$$

Where Δf_{3dB} is the difference between two frequencies f1 and f2 at half power beam width and f_r is the resonance frequency.

3.4.5 Device Damping:

Damping plays important role in dynamic mode. There are many types of damping, such as viscous, hysteresis, acoustic coupling, air pumping at joints, energy radiation to the soil, etc. Also, boundaries and bearings contribute damping in a structure. While in our micro flying robot device four types of damping are effective air flow damping, structural damping, squeeze film damping and damping due to anchor losses.

3.4.5.1 Air Flow Damping:

Air flow also cause the damping in the vibrating MEMS cantilever beam. The air flow damping ratio can be calculated by using the Kokubun et al's models[32]. He used Stokes' law to derive a damping coefficient for a cantilever beam oscillating at a frequency at $\boldsymbol{\omega}$.

$$\xi_n = 3\pi\mu b + \frac{3}{4}\pi b^2 \sqrt{2\mu\rho\omega} \tag{3.13}$$

Where μ and ρ is the viscosity and density of air and b is the width of the cantilever beam.

3.4.5.2 Structural Damping:

Internal friction in the resonating devices causes the energy dissipation and can be calculated by using the structural damping theory. The structural damping ratio can be calculated by equation 3.14

$$\xi_n = \frac{\eta_{avg}}{\omega_n} k \tag{3.14}$$

η_{avg} is the average structural damping coefficient of the silicon di oxide, aluminum and polysilicon, k is the cantilever beam stiffness coefficient and ω_n is the natural frequency.

3.4.5.3 Squeeze-film Damping Force:

In micro-structures when an oscillator is placed closed to a rigid body wall it experiences an air flow force due to the gap between the oscillating cantilever beam and the substrate, this new air flow force is called as the squeeze force which cause a damping in the micro-cantilever beam. The damping ratio for the nth mode can be given as in equation 3.15.

$$\xi_n = \frac{\mu {w_c}^2}{2\rho_b {g_o}^3 t_c \omega_n} \tag{3.15}$$

Where μ is the viscosity of air, the distance between the cantilever beam and the substrate is represented byg_o. ρ_b, t_c, w_c and ω_n is the density, thickness, width and the natural frequency of the cantilever beam.

3.4.5.4 Anchor Loss Damping:

Most of the anchor losses in any mechanical process occurs due to friction between the surfaces connected to each other firmly. The main cause of the anchor damping is due to the elastic vibration of the base plate. The dissipated energy per cycle of the oscillation can be calculated by modelling the substrate plate (base plate) as the elastic body. The damping ratio due to the anchor loss is given by equation 3.16.

$$\xi_1 = \frac{0.23h^3}{l^3} \tag{3.16}$$

Here h, l is the thickness and the length of the cantilever.

3.4.6 Resonance Frequency:

Resonance frequency (f_r) of the resonating device can be determined experimentally and theoretically. Intellisuite software is used to measure the resonance frequency of the cantilever and theoretically it is measured by using MATLAB. The resonance frequency values obtained from both by simulation and theoretical are very close. The resonance frequency can be derived by the Equation 3.17.

$$f_r = \frac{1}{2\pi}\sqrt{\frac{\left(\frac{Ew_b t_b{}^3}{4l_b{}^3}\right)}{\rho_{avg}(V_b)}} \tag{3.17}$$

Here l, w and t is the length, width and thickness of the cantilever beam. E is the Young's modulus and V_b is the volume of the cantilever beam.

3.5 Temperature of Device

The four beams and four polysilicon resistors in one wing of micro flying robot device each beam contains one poly silicon resistor connected with aluminum through via of tungsten. When AC current passes through the polysilicon and aluminum beams the temperature is produced due to the joule heating effect as already discussed. The change is electrical resistance due to temperature is measured in equation 3.2. due to applied potential across the ends of the beams the current starts passing from that structure and temperature in the structure is rises. This change in temperature is

measured using equation 3.18 and thermal resistivity of material is measured in equation 3.19.

$$\Delta T = \frac{I^2 R_{Th}}{L_b k} \quad (3.18)$$

Where

$$R_{Th} = \frac{L_b}{k w_b t_b} \quad (3.19)$$

In equation (3.13) and (3.14) ΔT is change in temperature, R_{Th} is thermal resistance of material, L_b is length of cantilever beam, k is conductivity of the material, w_b , t_b are width and length of cantilever beam.

3.6 Virtual Fabrication:

Micro flying robot in this research work is modeled and designed using MATLAB, Intellisuite and Layout editor software. Fabrication of the device is done in virtual environment of Intellisuite. This software contains many modules but for our device we use four of them which are given below.

1. Blueprint (Sketch/Mask)
2. Intelli Fab
3. Fab Sim
4. TEM Module

3.6.1 Blueprint:

Blue print Module is used for the sketching and creation of masks of the components or the layers used for the fabrication such as masking of wires, resistors, beams, via, connection pads etc. mask of the wing and complete layout shown in fig. 8. In legend metal 1,2,3 are aluminum metals, while vias are made of tungsten silicon is used for the base structure and SiO_2 is used for isolation between two layers.

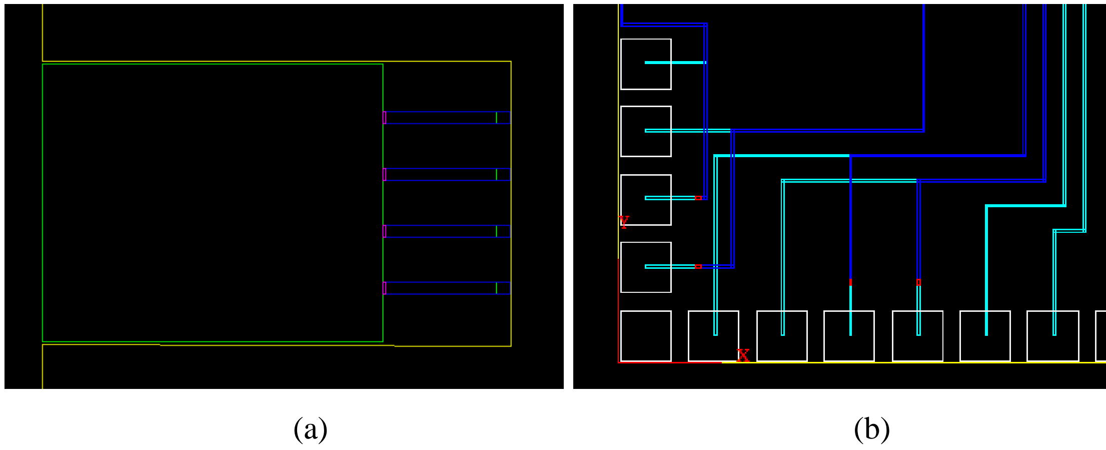

Fig 8: (a) Mask of wing attached with static part (b) Mask of wiring and connection pads

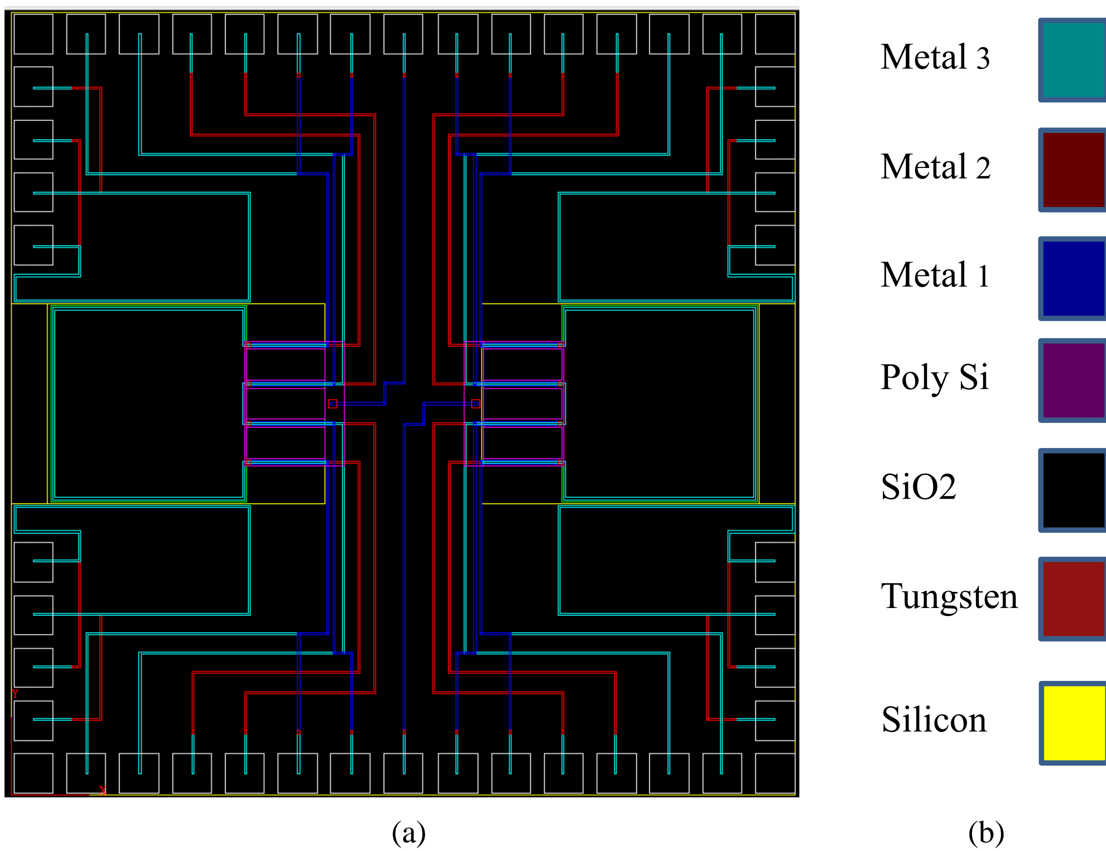

Fig 9: (a) Overall masks for the virtual fabrication (b) Legend

3.6.2 Intelli Fab:

Intelli Fab module is used for the virtual fabrication in that module we fabricate the device layer by layer as shown in fig. 10.

#	Type	Material	Process	Process ID	Process Option
G	Base				
1	Definition	Si	Czochralski	Generic	
2	Deposition	SiO2	LPCVD	TEOS	Conformal Deposition
3	Deposition	PolySi	LPCVD	SiH4	Conformal Deposition
4	Deposition	SiO2	LPCVD	TEOS	Conformal Deposition
G	Poly Silicon Beam				
5	Deposition	PolySi	LPCVD	SiH4	Conformal Deposition
6	Deposition	PR-AZ5214	Spin	001	Conformal Deposition
7	Exposure	UV	Contact	Suss	
8	Etch	PolySi	RIE	Cl2	Partial Etching
9	Etch	PR-AZ5214	Wet	1112A	Partial Etching
10	Deposition	SiO2	LPCVD	TEOS	Non-conformal Deposition
G	Al Beam				
11	Deposition	Al	Bulk	Standard	Conformal Deposition
12	Deposition	PR-AZ5214	Spin	001	Conformal Deposition
13	Exposure	UV	Contact	Suss	
14	Etch	Al	RIE	Cl2_BCl3	Partial Etching
15	Etch	PR-AZ5214	Wet	1112A	Partial Etching
16	Deposition	SiO2	LPCVD	TEOS	Conformal Deposition
G	VIA creation				
17	Deposition	PR-AZ5214	Spin	001	Conformal Deposition
18	Exposure	UV	Contact	Suss	
19	Etch	SiO2	RIE	CHF3_CF4	Etch Through
20	Exposure	UV	Contact	Suss	
21	Etch	SiO2	RIE	CHF3_CF4	Etch Through
22	Etch	PR-AZ5214	Wet	1112A	Partial Etching
23	Deposition	W	Bulk	Standard	Conformal Deposition
24	Deposition	PR-AZ5214	Spin	001	Conformal Deposition
25	Exposure	UV	Contact	Suss	
26	Etch	W	Wet	Dilute_Peroxide	Partial Etching
27	Etch	PR-AZ5214	Wet	1112A	Partial Etching
G	Al Beam				
28	Deposition	Al	Bulk	Standard	Conformal Deposition
29	Deposition	PR-AZ5214	Spin	001	Conformal Deposition
30	Exposure	UV	Contact	Suss	
31	Etch	Al	RIE	Cl2_BCl3	Partial Etching
32	Etch	PR-AZ5214	Wet	1112A	Partial Etching
G	Cutting for Mov...				
33	Deposition	PR-AZ5214	Spin	001	Conformal Deposition
34	Exposure	UV	Contact	Suss	
35	Etch	Si	DRIE	SF6_C4F8	Etch Through
36	Etch	SiO2	RIE	CHF3_CF4	Etch Through
37	Etch	PR-AZ5214	Wet	1112A	Partial Etching
38	Deposition	PR-AZ5214	Spin	001	Conformal Deposition
39	Exposure	UV	Contact	Suss	
40	Etch	PolySi	RIE	Cl2	Etch Through
41	Etch	SiO2	RIE	CHF3_CF4	Etch Through
42	Etch	PR-AZ5214	Wet	1112A	Partial Etching

Fig 10: Layers by layer device designing using masks for different layers

In first step silicon wafer of thickness 50µm and length width of 4000x4000 µm is used for base structure, then SiO_2 of thickness 0.3 µm is deposited on it using low pressure chemical vapor deposition (LPCVD) method, then poly silicon of thickness 0.3 µm is deposited using same LPCVD method. To create polysilicon resistor 100nm thick photoresist layer is deposited then mask of resistor is pasted on it and expose the device in ultra violet (UV) rays which removes the photoresist from unmasked area. Below unmasked polysilicon layer is now etched using reactive ion etching (RIE) method and after that photoresist also etched using wet etching. The polysilicon resistor beam is ready as shown in fig. 11.

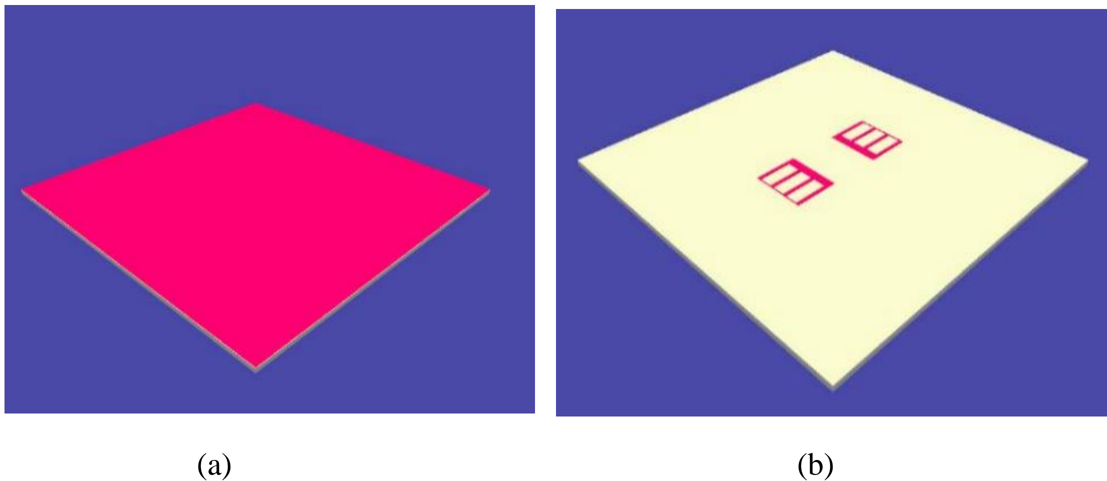

(a) (b)

Fig 11: (a) Polysilicon deposited layer (b) polysilicon resistor

SiO_2 is deposited for isolation via created by using the mask of via tungsten is deposited in via and aluminum beam is created in the same way as polysilicon beam is created as shown in fig. 12.

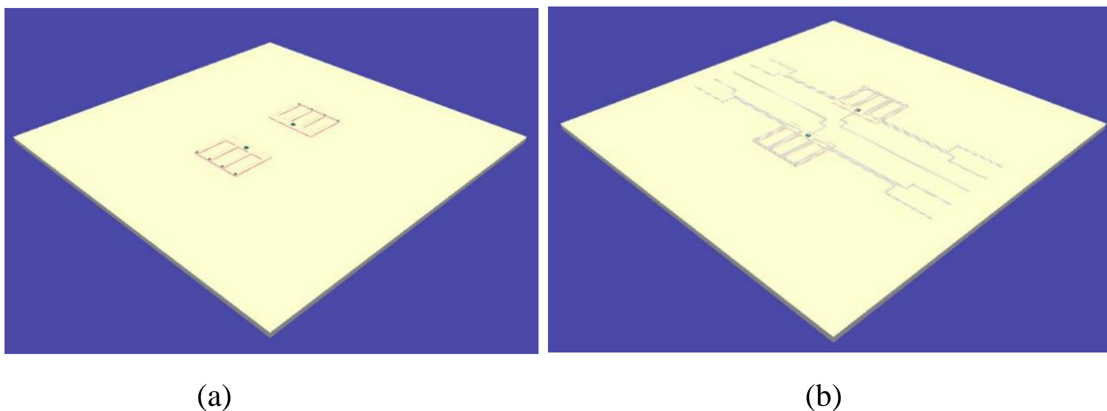

(a) (b)

Fig 12: (a) Creation VIA and deposition of tungsten in it (b) creation of aluminum first layer

At the end of designing silicon is etched from back side to free the wing for movement as shown in fig. 13

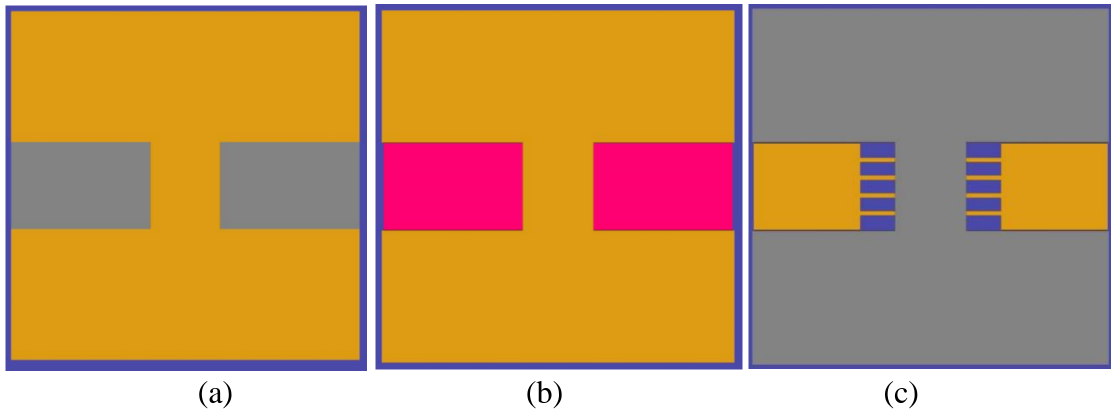

(a) (b) (c)

Fig 13: (a) Exposure for cutting of Si (b) Silicon etched (c) All unnecessary material etched to free Wing

3.6.3 Fab sim

Fab sim is the tool to visualize the virtual fabrication of device which is designed using the Intelli fab tool. Above figures 11, 12 and 13 are also captured from that tool. Cross sectional view of step by step manufacturing of the device is shown in fig. 14.

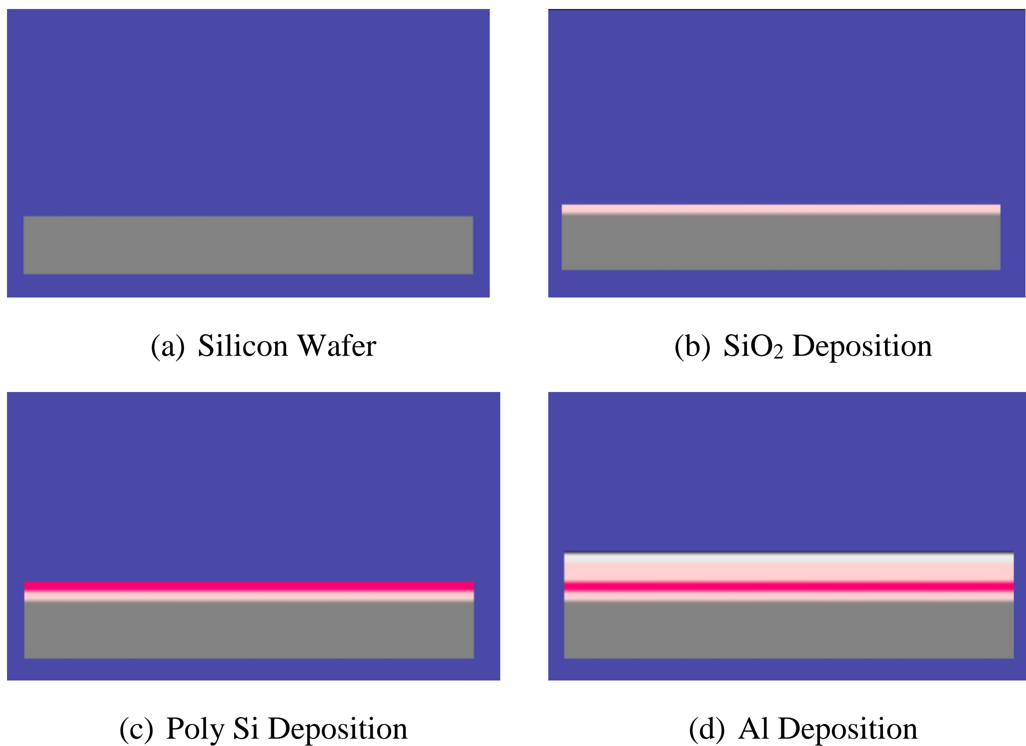

(a) Silicon Wafer (b) SiO_2 Deposition

(c) Poly Si Deposition (d) Al Deposition

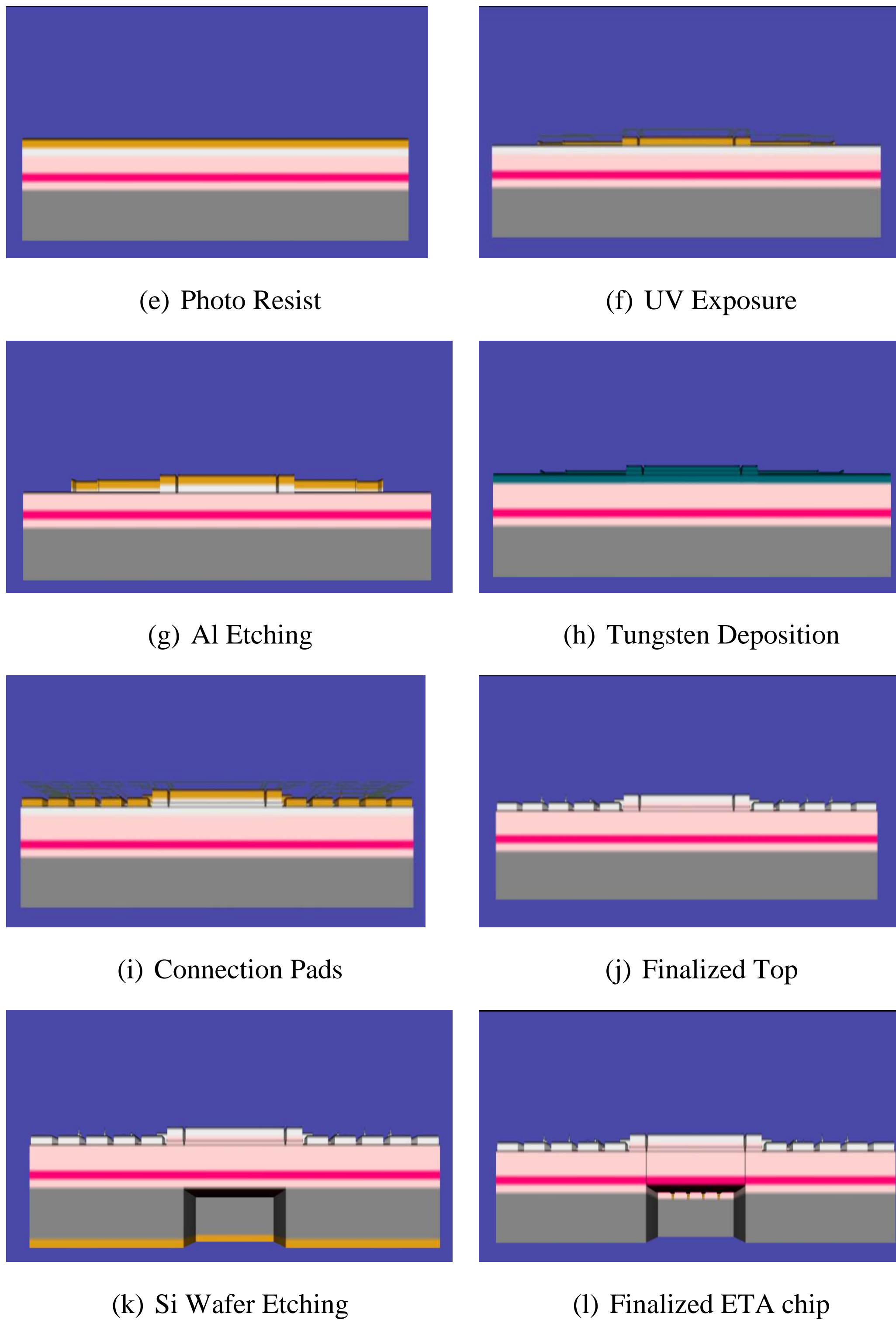

(e) Photo Resist

(f) UV Exposure

(g) Al Etching

(h) Tungsten Deposition

(i) Connection Pads

(j) Finalized Top

(k) Si Wafer Etching

(l) Finalized ETA chip

Fig 14. Cross sectional view of virtual fabrication in fab sim

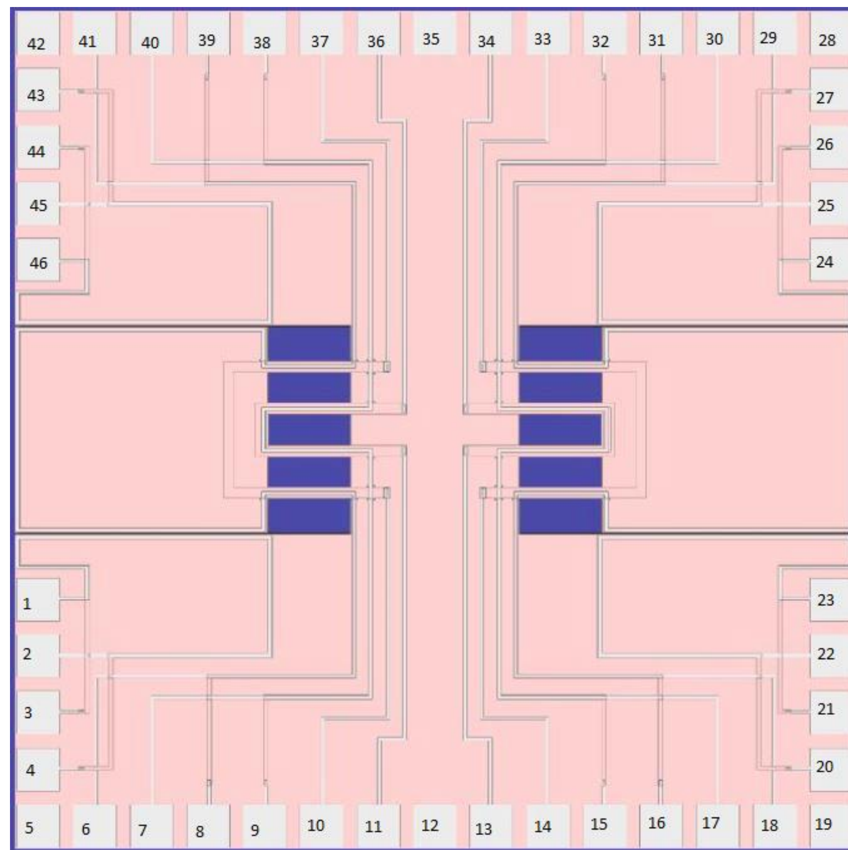

Fig 15 Micro flying robot chip based on CMOS-MEMS ETA

Pad#	Contact Pad Description	Function
10,11,12,36,37	Bimetallic actuator contacts in left wing	Lift and speed Control (Up / Down)
13,14,33,34,35	Bimetallic actuator contacts in right wing	
1,2,22,23	Controlling magnetic field in lower portion of static part at 2nd layer of Al	Generation of Magnetic Field for Movement
3,4,20,21	Controlling magnetic field in lower portion of static part at 3rd layer of Al	
24,25,45,46	Controlling magnetic field in upper portion of static part at 2nd layer of Al	
26,27,43,44	Controlling magnetic field in upper portion of static part at 3rd layer of Al	
6,7,40,41	Controlling magnetic field in left moveable part at 2nd layer	Direction Control (Left / Right)
8,9,38,39	Controlling magnetic field in left moveable part at 3rd layer	
17,18,29,30	Controlling magnetic field in right moveable part at 2nd layer	
15,16,31,32	Controlling magnetic field in right moveable part at 3rd layer	
5,19,28,42	Not used	

Table 4: ETA contact pad description

3.6.4 TEM Module

TEM stands for the Thermo-Electro-Mechanical analysis module. By using this module finite element analysis (FEA) done. The micro flying robot electro thermal actuator is analyzed by applying input voltages and measure the output in form of displacement, change in heat, change in current. Device also run in frequency mode to detect its natural frequency. One wing of the total chip is selected and meshed for analysis.

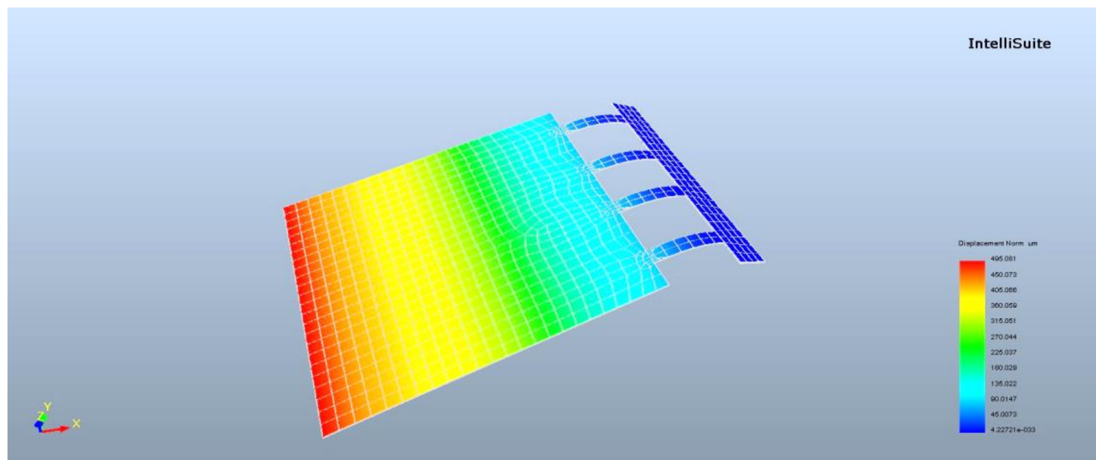

(a) Displacement at room temperature 25°C (µm)

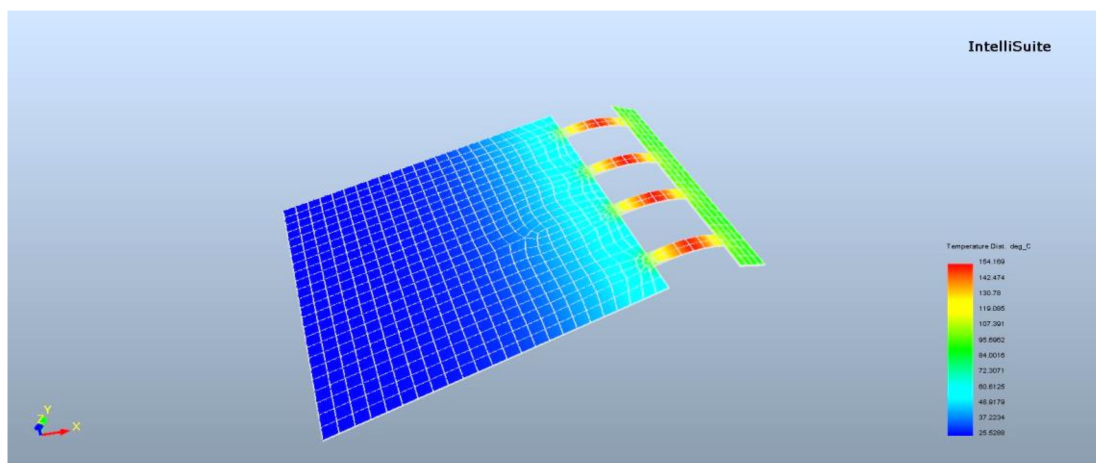

(b) Rise in temperature of ETA (°C)

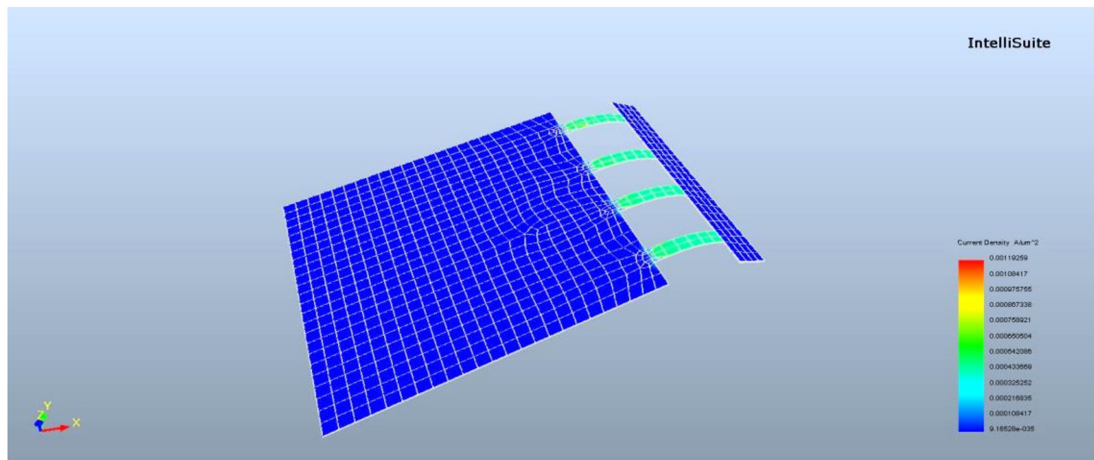

(c) Current Density (A/µm^2)

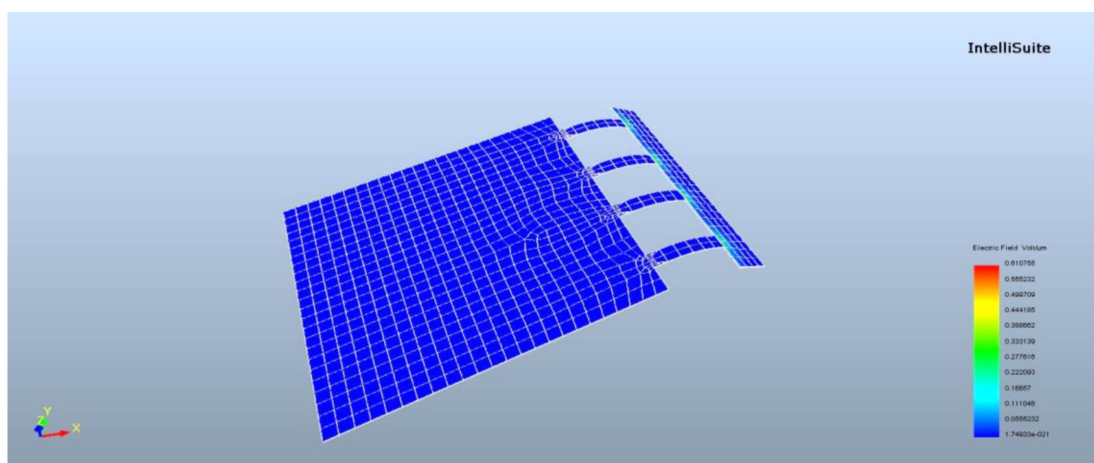

(d) Electric Field (V/µm)

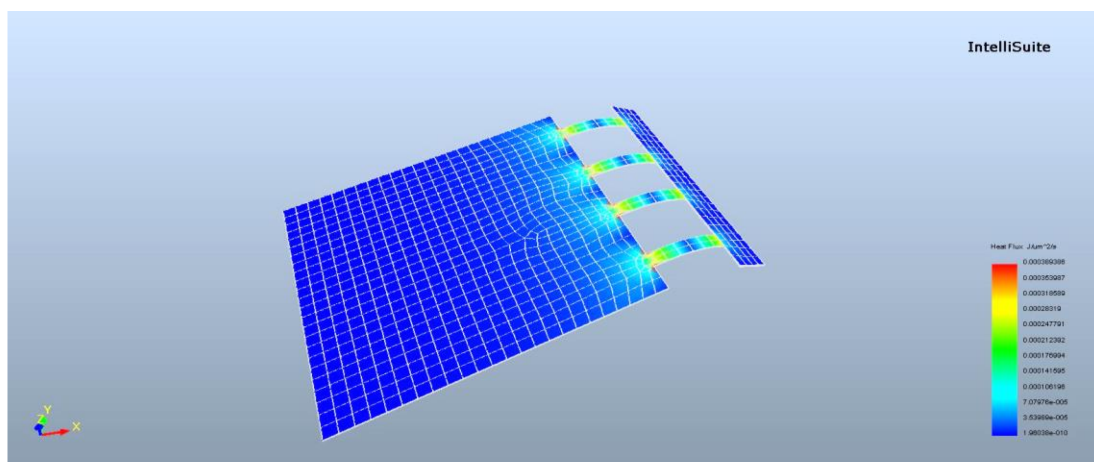

(e) Heat Flux (J/µm^2/s)

Fig 16: All above results are simulated in TEM module at 1V

Chapter 4

Results and Discussions

4.1 Results:

The results of the CMOS-MEMS electro-thermal actuator are obtained theoretically and by simulations. The theoretical analysis performed on MATLAB and then compared to the simulated results which are obtained from Intellisuite software. Following are the results which are obtained from simulation and relate with analytical results.

4.1.1 Connectivity Test:

In MEMS structure it is not easy to check whether all layers and wiring are intact with one another or not to check the connection potential is applied. The device starts drawing current when voltages applied at input side and with the increase in voltages current also increase this behavior shows that all the wiring and layers are intact and properly connected as shown in fig.17. The inverse of slope of shows the resistance of the device as shown in equation 3.20.

4.1.2 Uniformity in Layers:

The electric field distribution between the layers in not necessarily uniform in practically when fabricated. Ideally the thickness of every layer is uniformed but it is very difficult to control thickness of every layer. Minute difference of Nano or Pico meter (nm ~ pm) might be occurred in thickness of CMOS layers during micro fabrication process which shows non-uniform behavior. While in mathematical and simulated models the linear behavior of fig.18 shows that all parameters (thickness, length and width) are uniformly distributed.

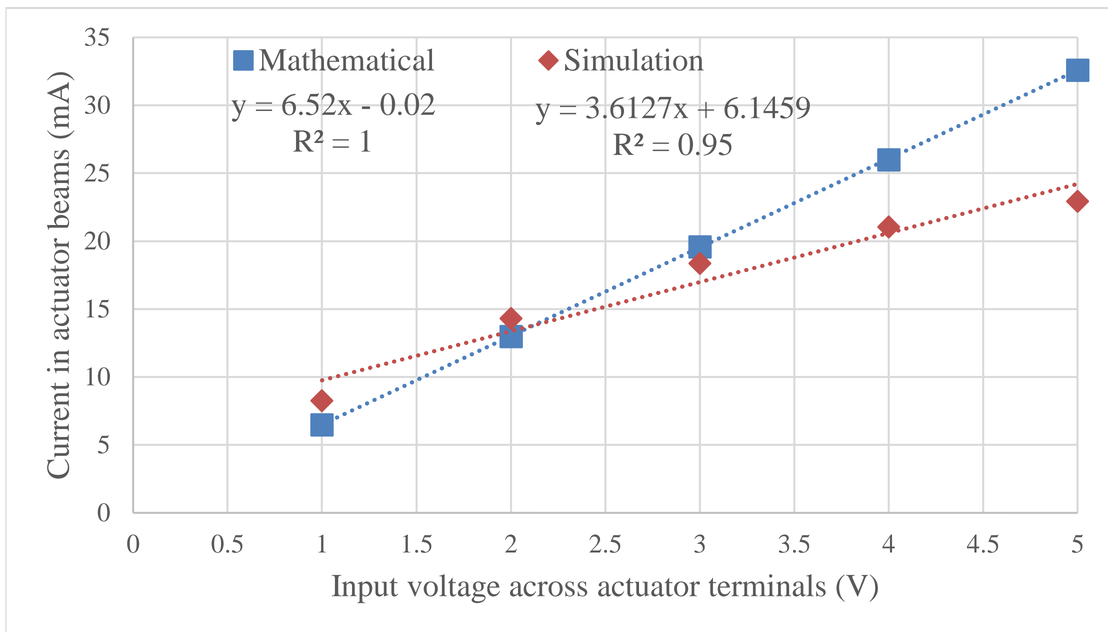

Fig 17: Input Voltages Vs Current in ETA beams

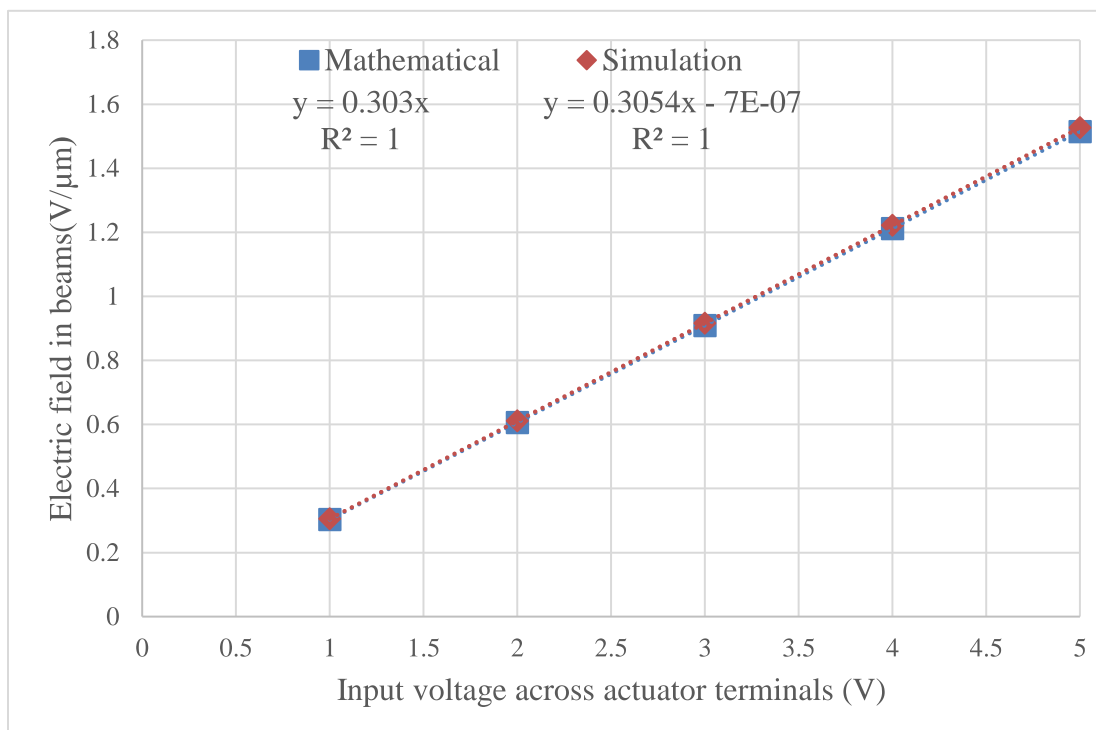

Fig 18: Applied Voltage Vs Electric Field

4.1.3 Power Consumption:

When input voltages increased at the input of the device power linearly increased. In below graph fig. 19 shows the consumption of power at different voltages. In our device we applying 0 to 5-volt maximum as we are bound to operate it within

CMOS limits because we design our chip compatible to CMOS-MEMS technology and in CMOS we have cap to use max 5V. If voltages increased beyond that limit device got damage.

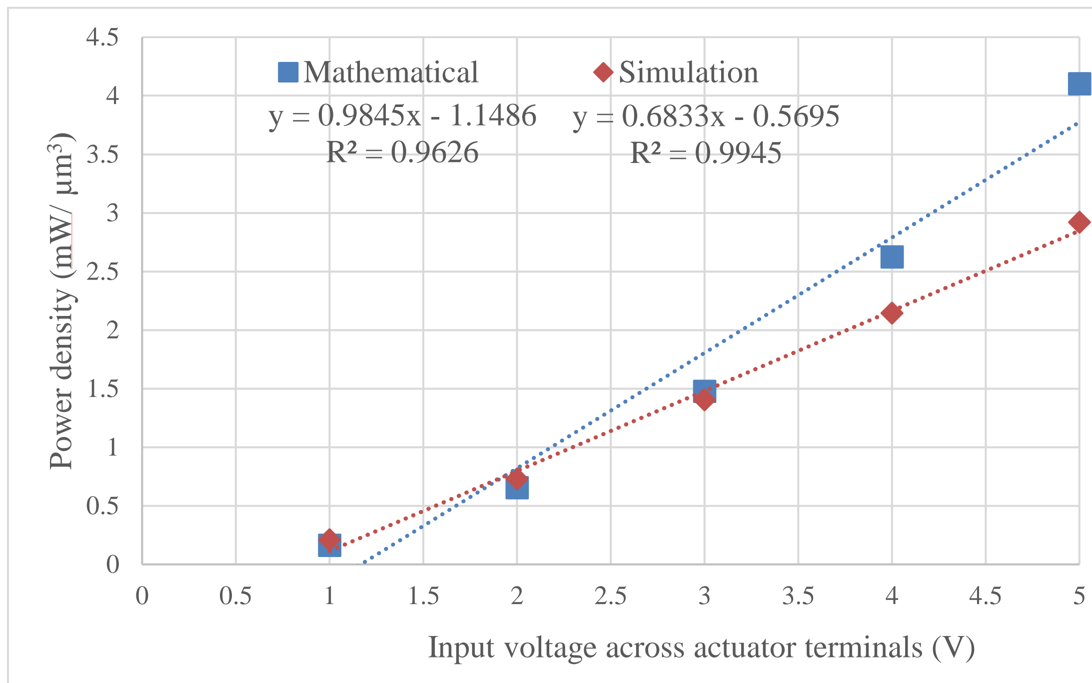

Fig 19: Input Voltages Vs Power Density

4.1.4 Heat Flux

When voltages increase the distribution of heat increased in the beam, the distribution of heat is shown in fig. 20. In structure where the density of the beam is more the resistance increase and due to increase in resistance the heat density will also increase at that point. As the area of beam is constant when voltages increased the speed of heat flow from unit area also increased.

4.1.5 Rise in Temperature:

When the input voltage is applied to the CMOS-MEMS ETA, the temperature of the beam rises due to the thermal resistance of the beams according to joules heating effect principle. Resistance of polysilicon is more than the aluminum that’s why more temperature rise occurred in polysilicon beam but both the beams are stacked and bind tightly with one another that’s way temperature rises uniformly in the beam. Temperature rise in the cantilever beams of ETA is shown in fig. 21.

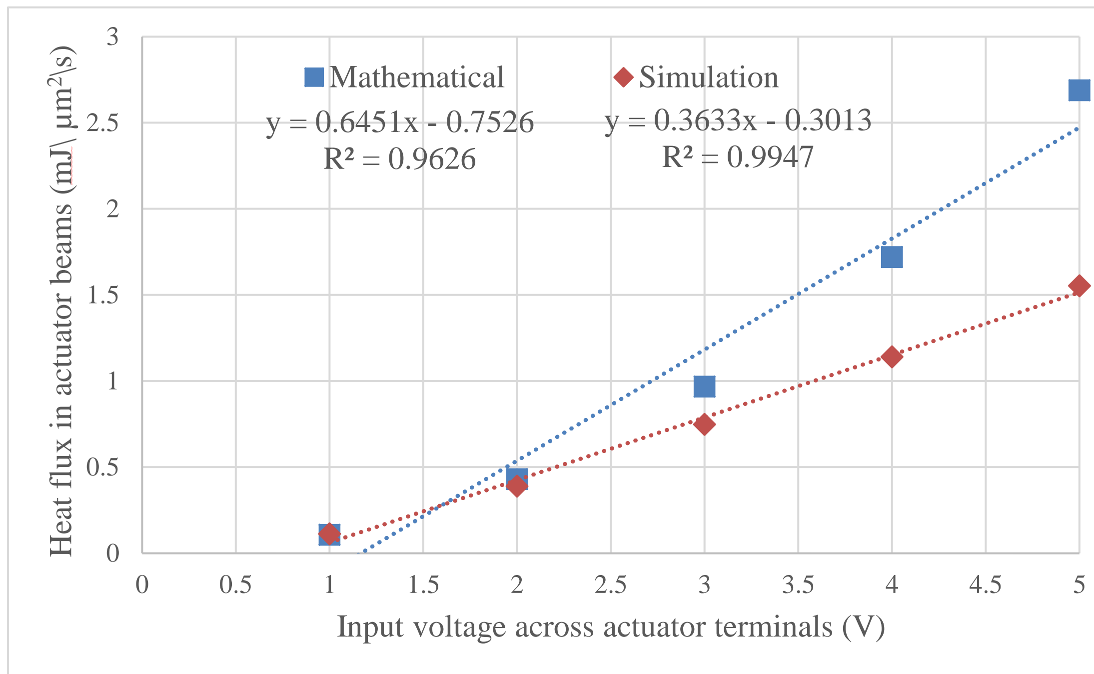

Fig 20: Input Voltages Vs Heat flux

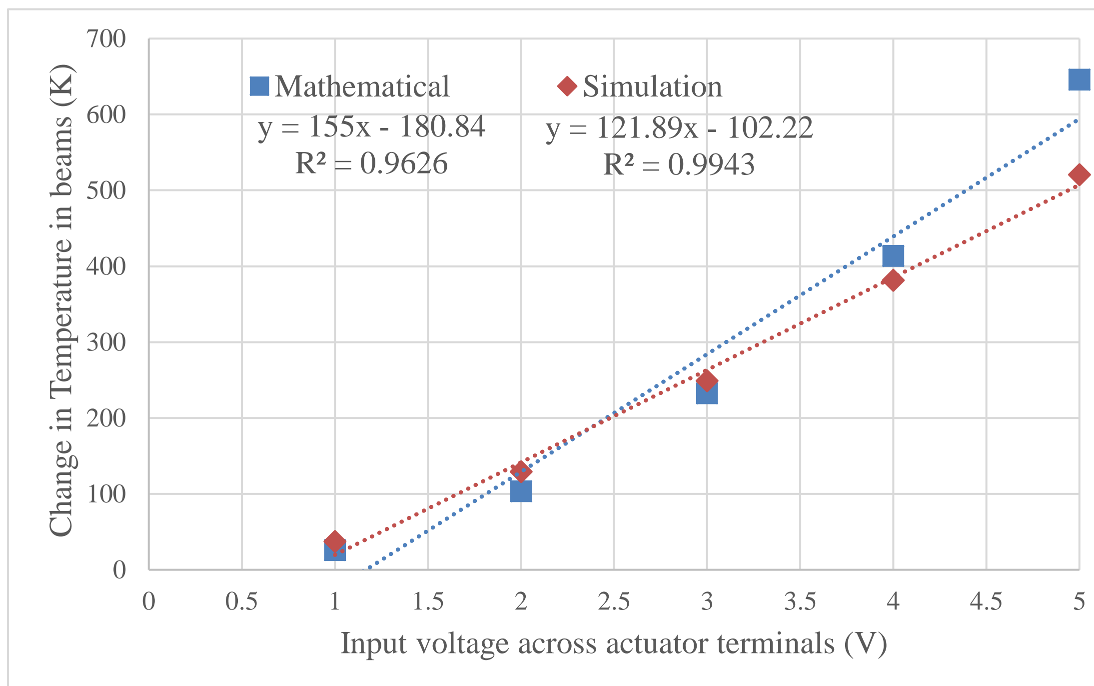

Fig 21: Applied Voltage Vs Change in Temperature

4.1.6 Change in Displacement

When the input voltage is applied to the contact pads of CMOS-MEMS electro-thermal actuator, the temperature of the beam rises due to the thermal resistance of the beams according to joules heating effect principle. When the temperature rises both polysilicon and aluminum expands as the CTE of aluminum is more than polysilicon it

shows more expansion. In ETA cantilever beam aluminum is on top and polysilicon is below the aluminum that's why displacement occurs towards the polysilicon and tip of proof mass which is attached with cantilever beams show bending downwards. The maximum displacement at tip on different voltages is shown in fig. 22.

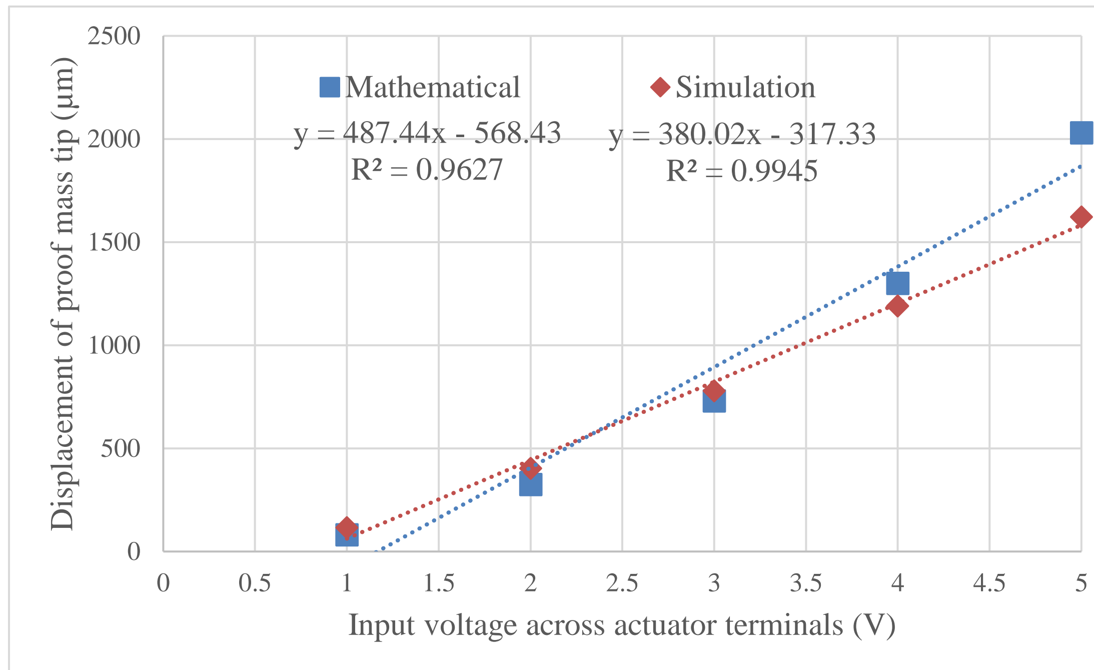

Fig 22: Input Voltage Vs Change in displacement at proof mass tip

4.1.7 Thermal Actuation Force:

There is no force at output side when potential is zero on CMOS-MEMS ETA. As when the voltages applied current passes through the device, maximum displacement produces at the tip of proof mass due to thermal expansion and temperature produced in the four legs of cantilevers beams. To get thermal actuation force the displacement of proof mass is multiplied with the spring or stiffness coefficient of the CMOS-MEMS device. The thermal actuation force shows the linear behavior because of the linear behavior of displacement in the proof mass as shown in fig. 23.

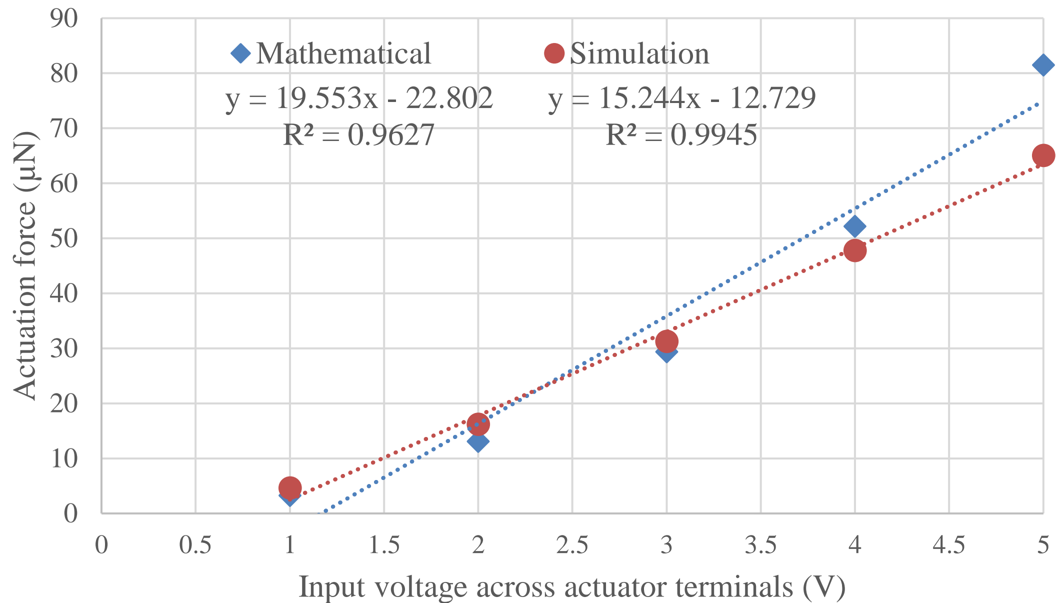

Fig 23: Applied Voltage Vs Thermal Actuation Force

4.1.8 Amplitude Vs Driving Frequency:

All above discussed results are in static mode, power consumption in static mode is more to maintain continues displacement DC signal is applied and

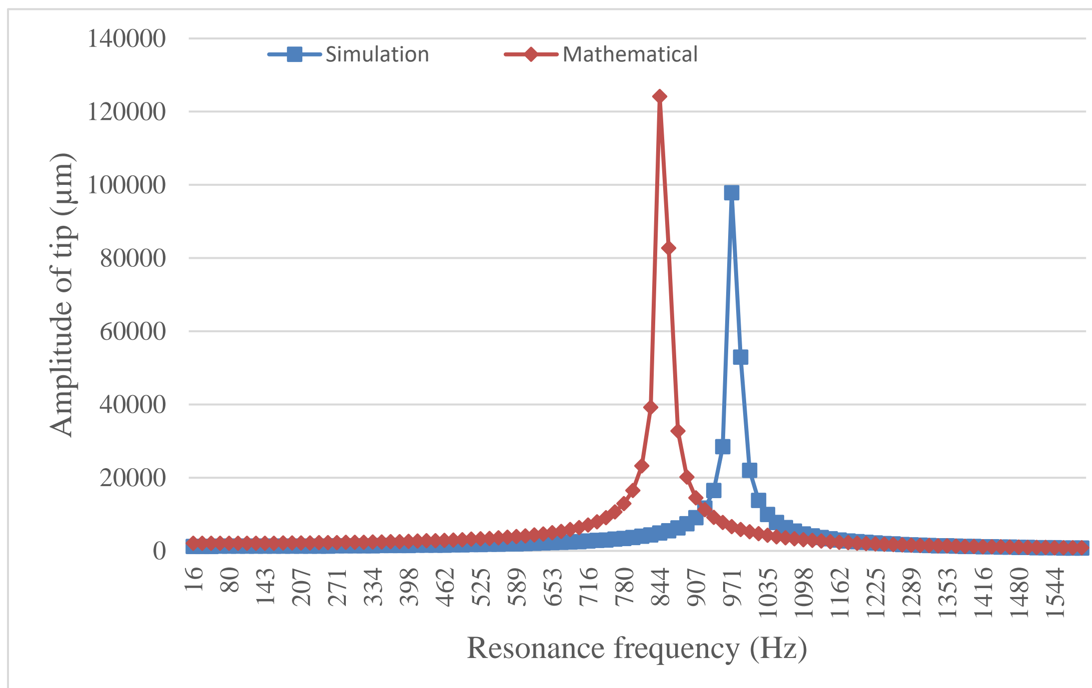

Fig 24: Amplitude Vs Driving Frequency in Dynamic Mode

displacement is smaller as compared to the dynamic mode. In dynamic mode the consumption of power is reduced and quality factor of the device is improved. When

AC signal is applied the device is operated at its resonance frequency and maximum amplitude is attained when its driving frequency becomes equal to its resonance frequency. The maximum amplitude of 124.15mm is obtained at the resonance frequency of 843Hz with driving force of 3.26µN mathematically. While in simulation maximum amplitude of 97.82mm is obtained at the resonance frequency of 970Hz with driving force of 4.67µN. The graph between the amplitude and driving frequency is shown in above figure.

Chapter 5

Conclusion and Future Work:

5.1 Conclusions:

This research work explains the modeling and design of CMOS-MEMS ETA used in micro flying robot. A bimorph cantilever beam structure is used for the electro-thermal actuator, and proof mass at the free end of cantilever beam is installed to increase its displacement and able to fly in air. The design is virtually fabricated in INTELLISUITE software by using CMOS-MEMS technique. Displacement of the device increases with the increase in voltage, proof mass size and beams length linearly. It is also noticed that the temperature of this device rises gradually in linear form as we increase the voltage. Device is optimized on the basis of its proof mass size, heat flux, temperature and displacement. 700µm**x**700µm proof mass is used for the wing. Power consumption of this device at 1V simulated is 8mW and 6.50mW at 1V mathematically. The thermal output force linearly changes as the input voltage changes. The maximum output thermal force is reported to be 81µN mathematically and 65.1µN in simulation at input voltage of 5V. The maximum amplitude of device is 124.15mm with the quality factor of 107.78 at the resonance frequency of 843Hz mathematically. While in simulation maximum amplitude of 97.82mm is obtained with the quality factor of 105.38 at the resonance frequency of 970Hz. The actuation force to drive the cantilever in dynamic mode is 3.26µN mathematically and 4.67µN in simulation. At 2V the mathematical and simulated results are approximately same, 28.6mW power is used at 2V for the displacement of 129µm.

5.2 Future Work:

The CMOS-MEMS device will be further improved in two aspects first is improvement in actuating mechanism and second is improvement in micro flying robot device in a whole.

5.2.1 Actuator:

Tilt angle of the wing will be controlled using electromagnetic actuation mechanism. Coil for electromagnetic mechanism is already embedded in design; secondly the temperature compensation circuit will be added to stable it from temperature variation effects (weather effects).

5.2.2 Micro Flying Robot:

Power of the flying robot will be harvested from on chip comb drives other power sources like solar can also be considered for increase in backup. Audio, Video, and communication features will be added for surveillance and reporting purpose. Gas sensors will be added for detection of life in hazardous situations.

Appendix I

Analytical Calculations:

$$\frac{1}{r} = \frac{6w_1w_2E_1E_2t_1t_2(t_1+t_2)(\alpha_1-\alpha_2)\Delta T}{(w_1E_1t_1^2)^2+(w_2E_2t_2^2)^2+2w_1w_2E_1E_2t_1t_2(2t_1^2+3t_1t_2+2t_1^2)}$$

$$F_T = \frac{Ewt^3d_l}{4l^3}$$

$$d = r - rcos\theta$$

$$\ddot{Z}+\gamma\dot{Z}+\ \omega^2 Z = \frac{F_o}{m}e^{j\omega_d t}$$

$$Y = \ \mathcal{R}e\{Z\}$$

$$Y = \mathcal{R}e\left\{\ddot{Z}+\gamma\dot{Z}+\ \omega^2 Z = \frac{F_o}{m}e^{j\omega_d t}\right\}$$

$$Y = m\ddot{Y}+b\dot{Y}+kY = F_T cos\omega_d t$$

$$Y_{SS}(t) = Acos\omega_d t + Bsin\omega_d t$$

$$\dot{Y_{SS}}(t) = \frac{d(Y_{SS}(t))}{dt} = -\omega_d Asin\omega_d t + \omega_d Bcos\omega_d t$$

$$\ddot{Y_{SS}}(t) = \frac{d^2(Y_{SS}(t))}{dt^2} = -\omega_d^2 Acos\omega_d t - \omega_d^2 Bsin\omega_d t$$

Substituting the values of $\ddot{X}_{SS}(t)$,$\dot{X}_{SS}(t)$,and $X_{SS}(t)$ in above Eq.

$$m\left(-\omega_d^2 Acos\omega_d t - \omega_d^2 Bsin\omega_d t\right) + b(-\omega_d Asin\omega_d t + \omega_d Bcos\omega_d t) + k(Acos\omega_d t + Bsin\omega_d t) = F_T cos\omega_d t$$

$$\left(-\omega_d^2 mA + \omega_d bB + kA\right)cos\omega_d t + \left(-\omega_d^2 mB - \omega_d bA + kB\right)sin\omega_d t = F_T cos\omega_d t$$

Comparing coefficient of $cos\omega_d t$ and $sin\omega_d t$, we get:

$$-\omega_d^2 mA + \omega_d bB + kA = F_T$$

$$-\omega_d^2 mB - \omega_d bA + kB = 0$$

By substituting following in above two system of equation:

$$\omega_0 = \sqrt{\frac{k}{m}} \quad \text{and} \quad \gamma = \frac{b}{m}$$

Solution of system of linear equation is:

$$A = \frac{\frac{F_T}{m}(\omega_o^2-\omega_d^2)}{\left(\omega_o^2-\omega_d^2\right)^2+(\gamma\omega_d)^2} \quad , \ B = \frac{\frac{F_T}{m}(\gamma\omega_d)}{\left(\omega_o^2-\omega_d^2\right)^2+(\gamma\omega_d)^2}$$

Thus the steady state solution of non-homogeneous 2nd order differential equation is obtained as:

$$Y_{SS} = \left\{\frac{\frac{F_T}{m}(\omega_o^2 - \omega_d^2)}{(\omega_o^2 - \omega_d^2)^2 + (\gamma\omega_d)^2}\right\} cos\omega_d t + \left\{\frac{\frac{F_T}{m}(\gamma\omega_d)}{(\omega_o^2 - \omega_d^2)^2 + (\gamma\omega_d)^2}\right\} sin\omega_d t$$

$$\nabla A = \sqrt{A^2 + B^2}$$

$$\nabla A = \sqrt{\left[\frac{\frac{F_T}{m}(\omega_o^2 - \omega_d^2)}{(\omega_o^2 - \omega_d^2)^2 + (\gamma\omega_d)^2}\right]^2 + \left[\frac{\frac{F_T}{m}(\gamma\omega_d)}{(\omega_o^2 - \omega_d^2)^2 + (\gamma\omega_d)^2}\right]^2}$$

$$\nabla A = \sqrt{\frac{\left(\frac{F_T}{m}\right)^2 [(\omega_o^2 - \omega_d^2)^2 + (\gamma\omega_d)^2]}{[(\omega_o^2 - \omega_d^2)^2 + (\gamma\omega_d)^2]^2}}$$

$$\nabla A = \frac{F_T/_m}{\sqrt{(\omega_o^2 - \omega_d^2)^2 + (\gamma\omega_d)^2}} \quad \text{where } F_T = \frac{Ewt^3 d_l}{4l^3}$$

Thus the output differential amplitude (∇A) is:

$$\nabla A = \frac{\left(\frac{Ewt^3 d_l}{4l^3}\right)/_m}{\sqrt{(\omega_o^2 - \omega_d^2)^2 + (\gamma\omega_d)^2}}$$

$$\gamma = 2\xi\omega_o = \frac{b}{m}$$

$$\nabla A_{max} = \frac{F_T}{m\omega_o\gamma}$$

$$\nabla A_{max} = \frac{\left(\frac{Ewt^3 d_l}{4l^3}\right)}{m\omega_o\gamma}$$

$$tan\delta = \frac{B}{A} = \frac{\left(\frac{\frac{F_o}{m}(\gamma\omega_d)}{(\omega_o^2 - \omega_d^2)^2 + (\gamma\omega_d)^2}\right)}{\left(\frac{\frac{F_o}{m}(\omega_o^2 - \omega_d^2)}{(\omega_o^2 - \omega_d^2)^2 + (\gamma\omega_d)^2}\right)}$$

$$tan\delta = \frac{\gamma\omega_d}{\omega_o^2 - \omega_d^2}$$

$$\delta = tan^{-1}\left(\frac{\gamma\omega_d}{\omega_o^2 - \omega_d^2}\right)$$

$$\xi = \frac{\gamma}{2\omega_o} = \frac{1}{2Q} = \frac{b}{2m\omega_o} = \frac{b}{b_c} \quad \text{Where } b_c = 2\sqrt{km}$$

$$Q = \frac{\omega_o}{\gamma} = \frac{f_r}{\Delta f_{3dB}} = \frac{m\omega_o}{b} = \frac{1}{2\xi}$$

$$k_b = \frac{EW_b {H_b}^3}{4{L_b}^3}$$

$$f = \frac{1}{T} = \frac{\omega_o}{2\pi}$$

$$f_r = \frac{1}{2\pi}\sqrt{\frac{k_b}{m}}$$

$$f_r = \frac{1}{2\pi}\sqrt{\frac{EW_b {H_b}^3}{4{L_b}^3 V_b \rho_{avg}}}$$

$$\rho_{avg} = \frac{\rho_{SiO2} + \rho_{H-poly} + \rho_{Al}}{3}$$

$$R = \rho\frac{l}{A}$$

$$R(t) = R_o\{1 + \alpha(t - t_o)\}$$

Appendix II

MATLAB CODE for Resonance Frequency:

```
%% Design and Simulation of Electro Thermal Actuator for micro flying
robot
clear all
close all
clc

%%Input Parameter
V=1;                                    %Voltage
V_array=[1 2 3 4 5];                    %Voltage array

%% Material Properties
% _1 represents to Si
% _2 represents to SiO2
% -3 represents to Poly Silicon
% _4 represents to Aluminum
% _5 represents to Tungsten

%Densities      kg/m^3
pd_1=2328;                    %Density of Silicon
pd_2=2270;                    %Density of Silicon dioxide
pd_3=2300;                    %Density of Poly Silicon
pd_4=2700;                    %Density of Aluminum
pd_5=19250;                   %Density of Tungsten
pd_avg=(pd_2+pd_3+pd_4+pd_5)/4;
                              %average density

%Young's Modulus   Pa
E_1=190e9;                    %Young's Modulus of Silicon
E_2=160e9;                    %Young's Modulus of Silicon dioxide
E_3=169e9;                    %Young's Modulus of Poly Silicon
E_4=70e9;                     %young's Modulus of Aluminum
E_5=410e9;                    %young's Modulus of Tungsten
E_avg=(E_2+E_3+E_4+E_5)/4;    %Average young's Modulus

% Poisson Ratio     #
PR_1=0.278;                   %Poisson Ratio of Silicon
PR_2=0.226;                   %Poisson Ratio of Silicon dioxide
PR_3=0.42;                    %Poisson Ratio of Poly Silicon
PR_4=0.33;                    %Poisson Ratio of Aluminum
PR_5=0.28;                    %Poisson Ratio of Tungsten

%Co-eefficent of thermal expansion 1/K
a_1=32e-7;                    %CTE Ratio of Silicon
a_2=29e-7;                    %CTE Ratio of Silicon dioxide
a_3=29.05e-7;                 %CTE Ratio of Poly Silicon
a_4=230e-7;                   %CTE Ratio of Aluminum
a_5=45e-7;                    %CTE Ratio of Tungsten

%Thermal Co-efficient of resistance #
TCR_3=2.1e-3;                 %TCR of Poly Silicon
TCR_4=4.29e-3;                %TCR of Aluminium
```

```
TCR_5=4.5e-5;                 %TCR of Tungsten

%Thermal Conductivity W/m.K
tcon_1=157;                   %Thermal cond of Silicon
tcon_2=150;                   %Thermal cond of Silicon dioxide
tcon_3=200;                   %Thermal cond of Poly Silicon
tcon_4=236;                   %Thermal cond of Aluminum
tcon_5=187;                   %Thermal cond of Tungsten
tcon_avg=(tcon_2+tcon_3+tcon_4+tcon_5)/4;

%Specific Heat      J/kg/K
Sh_1=712;                     %Specific Heat of Silicon
Sh_2=745;                     %Specific Heat of Silicon dioxide
Sh_3=710;                     %Specific Heat of Poly Silicon
Sh_4=898;                     %Specific Heat of Aluminum
Sh_5=710;                     %Specific Heat of Tungsten

%Dielectric Constant #
d_1=1;                        %Dielectric # of Silicon
d_2=11.9;                     %Dielectric # of Silicon dioxide
d_3=1;                        %Dielectric # of Poly Silicon
d_4=10.8;                     %Dielectric # of Aluminum
d_5=11.9;                     %Dielectric # of Tungsten

%Resistivity      ohm.m
p_1=0.023;                    %Resistivity of Silicon
p_2=1.1e15;                   %Resistivity of Silicon dioxide
p_3=9.2e-6;                   %Resistivity of Poly Silicon
p_4=2.71e-8;                  %Resistivity of Aluminum
p_5=5.6e-8;                   %Resistivity of Tungsten
p_avg=(p_3+p_4)/2;            %Average resistivity of conducting beam

%% dimensions of Actuator
%Thickness m
t_1=1e-6;                     %Thickness of Silicon
t_2=0.3e-6;                   %Thickness of Silicon dioxide
t_3=0.3e-6;                   %Thickness of Poly Silicon
t_4=0.624e-6;                 %Thickness of Aluminum
t_5=20e-6;                    %Thickness of Tungsten
t_b=t_2+t_3+t_4;              %Beam Thickness

%Width of Beams m
w_1=0e-6;                     %Width of Silicon Beam
w_2=40e-6;                    %Width of Silicon Dioxide Beam
w_3=40e-6;                    %Width of Polysilicon Beam
w_4=40e-6;                    %Width of Aluminum Beam
w_5=10e-6;                    %Width of Tungsten Beam

%Length of Beams m
l_1=0e-6;                     %Length of Silicon Beam
l_2=200e-6;                   %Length of Silicon Dioxide Beam
l_3=200e-6;                   %Length of Polysilicon Beam
l_4=200e-6;                   %Length of Aluminum Beam
l_5=1.074e-6;                 %Length of Tungsten Beam
l_r=l_3+l_4+.3e-6;            %Length of total resistive beam
L=3.30e-6;                    %Length for Electric Field


%Proof mass Profile
l_p=700e-6;                   %Length of Proof mass
```

```
w_p=700e-6;                     %Width of proof mass
t_p=1.224e-6;                   %Thickness of proof mass
l_t=900e-6;                     %Length of Beam with Proof mass m

%Area of resistor m^2
A_r=t_3*w_3;                    %Area of resistor

%Volume of Used materials m^3
V_2=t_2*(l_2*w_2-t_5*w_5);      %Volume of SiO2 in Beam
V_3=t_3/2*(l_3*w_3-t_5*w_5)+t_3/2*(l_3*w_3);
                                %Volume of Polysilicon in Beam
V_4=t_4*(l_4*w_4-t_5*w_5);      %Volume of Aluminum in Beam
V_5=t_5*l_5*w_5;                %Volume of Tungsten in Beam
V_p=(l_p*t_p*w_p);              %Volume of SiO2 in Proof mass

%Mass of single beam kg
m_1=(w_1*t_1*l_1)*pd_1;         %Mass of Silicon in a Beam
m_2=(w_2*t_2*l_2)*pd_2;         %Mass of Silicon dioxide in a Beam
m_3=(w_3*t_3*l_3)*pd_3;         %Mass of Polysilicon in a Beam
m_4=(w_4*t_4*l_4)*pd_4;         %Mass of Aluminum in a Beam
m_5=(w_5*t_5*l_5)*pd_5;         %Mass of Tungsten in a Beam
m_p=(l_p*t_p*w_p)*pd_2;         %Mass of Proffmass
M=m_2+m_3+m_4+m_5+m_p;          %Mass of Beam with proffmass

%Thermal Capacitance J/K
Ct_2=Sh_2*m_2;                  %Thermal capacitance of SiO2
Ct_3=Sh_3*m_3;                  %Thermal capacitance of polysilicon
Ct_4=Sh_4*m_4;                  %Thermal capacitance of Aluminum

%Temperature K
T_1=273.15;
T_2=273.15;
T_3=273.15;
T_4=273.15;
T_5=273.15;
Tr=293;                         %Room temperature

%% Spring Constant or Stiffness N.m
N=4;                            %Total numbers of beams
ky=(((E_4*w_4*(t_b)^3)/(l_4)^3)/4)/N;
                                %Spring constant

%% Effective Mass kg
M_2=pd_2*V_2;                   %Mass of SiO2 in Beam
M_A=pd_2*(1.5568e-13);          %Mass of SiO2 in Anchor
M_p=pd_2*V_p;                   %Mass of SiO2 in Proof mass
M_3=pd_3*V_3;                   %Mass of Polysilicon in Beam
M_4=pd_4*V_4;                   %Mass of Aluminum in Beam
M_5=pd_5*V_5;                   %Mass of Tungsten in Beam
M=pd_avg*(200e-6*40e-6*1.224e-6)+m_p;
                                %Average mass of wing

%% Resonance Frequency Hz
wn=sqrt(ky/M);                  %Angular Resonance frequency
fr=wn/(2*pi);                   %Resonance Frequency
```

MATLAB CODE for Damping, Damping Ratio and Quality Factor:

```
%% Damping, Damping Ratio and Quality Factor
clear all
close all
clc

%% Dimensions of Actuator
%Thickness      m
t_1=1e-6;                    %Thickness of Silicon
t_2=0.3e-6;                  %Thickness of Silicon dioxide
t_3=0.3e-6;                  %Thickness of Poly Silicon
t_4=0.624e-6;                %Thickness of Aluminum
t_5=20e-6;                   %Thickness of Tungsten
t_b=t_2+t_3+t_4;             %Beam Thickness

%Width of Beams m
w_1=0e-6;                    %Width of Silicon Beam
w_2=40e-6;                   %Width of Silicon Dioxide Beam
w_3=40e-6;                   %Width of Polysilicon Beam
w_4=40e-6;                   %Width of Aluminum Beam
w_5=10e-6;                   %Width of Tungsten Beam

%Length of Beams    m
l_1=0e-6;                    %Length of Silicon Beam
l_2=200e-6;                  %Length of Silicon Dioxide Beam
l_3=200e-6;                  %Length of Polysilicon Beam
l_4=200e-6;                  %Length of Aluminum Beam
l_5=1.074e-6;                %Length of Tungsten Beam

%Proof mass Profile
l_p=700e-6;                  %Length of Proof mass
w_p=700e-6;                  %Width of proof mass
t_p=1.224e-6;                %Thickness of proof mass
l_t=900e-6;                  %Length of Beam with Proof mass m

%% Material Properties
%Densities      kg/m^3
pd_1=2328;                   %Density of Silicon
pd_2=2270;                   %Density of Silicon dioxide
pd_3=2300;                   %Density of Poly Silicon
pd_4=2700;                   %Density of Aluminum
pd_5=19250;                  %Density of Tungsten
pd_avg=(pd_2+pd_3+pd_4+pd_5)/4;
                             %average density

%Young's Modulus    Pa
E_1=190e9;                   %Young's Modulus of Silicon
E_2=160e9;                   %Young's Modulus of Silicon dioxide
E_3=169e9;                   %Young's Modulus of Poly Silicon
E_4=70e9;                    %Young's Modulus of Aluminum
E_5=410e9;                   %Young's Modulus of Tungsten
E_avg=(E_2+E_3+E_4+E_5)/4;   %Average young's Modulus

%Volume of Used materials m^3
V_2=t_2*(l_2*w_2-t_5*w_5)    %Volume of SiO2 in Beam
V_3=t_3/2*(l_3*w_3-t_5*w_5)+t_3/2*(l_3*w_3);
                             %Volume of Polysilicon in Beam
```

```
V_4=t_4*(l_4*w_4-t_5*w_5);      %Volume of Aluminum in Beam
V_5=t_5*l_5*w_5;                %Volume of Tungsten in Beam
V_p=(l_p*t_p*w_p);              %Volume of SiO2 in Proof mass

%Mass of single beam kg
m_1=(w_1*t_1*l_1)*pd_1;         %Mass of Silicon in a Beam
m_2=(w_2*t_2*l_2)*pd_2;         %Mass of Silicon dioxide in a Beam
m_3=(w_3*t_3*l_3)*pd_3;         %Mass of Polysilicon in a Beam
m_4=(w_4*t_4*l_4)*pd_4;         %Mass of Aluminum in a Beam
m_5=(w_5*t_5*l_5)*pd_5;         %Mass of Tungsten in a Beam
m_p=(l_p*t_p*w_p)*pd_2;         %Mass of Proof mass
M=m_2+m_3+m_4+m_5+m_p;          %Mass of Beam with proof mass

%% Spring Constant or Stiffness N.m
N=4;                      %Total numbers of beams
ky=(((E_4*w_4*(t_b)^3)/(l_4)^3)/4)/N;

%% Effective Mass   kg
M_2=pd_2*V_2;                   %Mass of SiO2 in Beam
M_A=pd_2*(1.5568e-13);          %Mass of SiO2 in Anchor
M_p=pd_2*V_p;                   %Mass of SiO2 in Proof mass
M_3=pd_3*V_3;                   %Mass of Polysilicon in Beam
M_4=pd_4*V_4;                   %Mass of Aluminum in Beam
M_5=pd_5*V_5;                   %Mass of Tungsten in Beam
M=pd_avg*(200e-6*40e-6*1.224e-6)+m_p;
                                %Average mass of wing

%% Resonance Frequency Hz
wn=sqrt(ky/M);                  %Angular Resonance frequency

%% Damping
g_o=50e-6;                %Distance b/w cantilever and the substrate
u_a=1.81e-15;             %Viscosity of air
n_al=17.59e-6;            %Damping coefficient of aluminum (17.59kg/s)
pd_air=1.225;             %Density of Air in kg/m^3

%Air Flow Damping
D_air=(3*pi*(u_a)*(w_3))+((3/4)*pi*(w_3)^2*sqrt(2*u_a*pd_air*wn));

%Structural Damping
D_struc=(n_al/wn)*ky;

%Squeeze Film Damping
D_sque=(u_a)*(w_3)/(2*(pd_avg)*(g_o)^3*(t_b)*wn);

%Anchor Loss Damping
D_anchor=(0.23*(t_b)^3)/(l_3)^3;

%Total Damping
b=D_air+D_struc+D_sque+D_anchor;      %Damping
gema=b/M;                             %Damping Constant
zeta=gema/(2*wn);                     %Zeta

%Quality Factor
Q=(wn)/gema;
```

MATLAB CODE for ETA Displacement and Thermal Force:

```
%% ETA Displacement and Thermal Force
clear all
close all
clc

%%Input Parameter
V=1;                          %Voltage
V_array=[1 2 3 4 5];          %Voltage array

%% Dimensions of Actuator
%Thickness      m
t_1=1e-6;                     %Thickness of Silicon
t_2=0.3e-6;                   %Thickness of Silicon dioxide
t_3=0.3e-6;                   %Thickness of Poly Silicon
t_4=0.624e-6;                 %Thickness of Aluminum
t_5=20e-6;                    %Thickness of Tungsten
t_b=t_2+t_3+t_4;              %Beam Thickness

%Width of Beams m
w_1=0e-6;                     %Width of Silicon Beam
w_2=40e-6;                    %Width of Silicon Dioxide Beam
w_3=40e-6;                    %Width of Polysilicon Beam
w_4=40e-6;                    %Width of Aluminum Beam
w_5=10e-6;                    %Width of Tungsten Beam

%Length of Beams    m
l_1=0e-6;                     %Length of Silicon Beam
l_2=200e-6;                   %Length of Silicon Dioxide Beam
l_3=200e-6;                   %Length of Polysilicon Beam
l_4=200e-6;                   %Length of Aluminum Beam
l_5=1.074e-6;                 %Length of Tungsten Beam
l_r=l_3+l_4+.3e-6;            %Length of total resistive beam


%Proof mass Profile
l_p=700e-6;                   %Length of Proof mass
w_p=700e-6;                   %Width of proof mass
t_p=1.224e-6;                 %Thickness of proof mass
l_t=900e-6;                   %Length of Beam with Proof mass m

%Area of resistor m^2
A_r=t_3*w_3;                  %Area of resistor

%% Material Properties
%Thermal Conductivity W/m.K
tcon_1=157;                   %Thermal cond of Silicon
tcon_2=150;                   %Thermal cond of Silicon dioxide
tcon_3=200;                   %Thermal cond of Poly Silicon
tcon_4=236;                   %Thermal cond of Aluminum
tcon_5=187;                   %Thermal cond of Tungsten
tcon_avg=(tcon_2+tcon_3+tcon_4+tcon_5)/4;

%Young's Modulus    Pa
E_1=190e9;                    %Young's Modulus of Silicon
E_2=160e9;                    %Young's Modulus of Silicon dioxide
E_3=169e9;                    %Young's Modulus of Poly Silicon
E_4=70e9;                     %Young's Modulus of Aluminum
```

```
E_5=410e9;                    %Young's Modulus of Tungsten
E_avg=(E_2+E_3+E_4+E_5)/4;    %Average young's Modulus

%Co-efficient of thermal expansion 1/K
a_1=32e-7;                    %CTE Ratio of Silicon
a_2=29e-7;                    %CTE Ratio of Silicon dioxide
a_3=29.05e-7;                 %CTE Ratio of Poly Silicon
a_4=230e-7;                   %CTE Ratio of Aluminum
a_5=45e-7;                    %CTE Ratio of Tungsten

%Resistivity    ohm.m
p_1=0.023;                    %Resistivity of Silicon
p_2=1.1e15;                   %Resistivity of Silicon dioxide
p_3=9.2e-6;                   %Resistivity of Poly Silicon
p_4=2.71e-8;                  %Resistivity of Aluminum
p_5=5.6e-8;                   %Resistivity of Tungsten
p_avg=(p_3+p_4)/2;            %Average resistivity of conducting beam

%% Spring Constant or Stiffness N.m
N=4;                          %Total numbers of beams
ky=(((E_4*w_4*(t_b)^3)/(l_4)^3)/4)/N;

%% Changings in Electro-thermal actuator
%Thermal resistance K/W
Rth_2=(1/tcon_2)*(t_2/(w_2*l_2));
Rth_3=(1/tcon_3)*(t_3/(w_3*l_3));
Rth_4=(1/tcon_4)*(l_4/(w_4*t_4));
Rth=Rth_2+Rth_3+Rth_4;

%Current        A
I=((1/p_avg)*V*A_r/l_r);      %Current A

I_M=[];
for i=1:1:5
    I_M=[I_M ((1/p_avg)*V_array(i)*A_r/l_r)];
end

%Change in Temperature  K
delT=(I^2*Rth)/(l_3*tcon_3);
delT_M=[];
for i=1:1:5
delT_M=[delT_M (I_M(i)^2*Rth)/(l_3*tcon_3)];
end

%Radius of curvature of arc m
r1=6*t_3*t_4*E_3*E_4*t_3*t_4*(t_3+t_4)*(a_4-a_3)*delT;
r2=(w_3*E_3*t_3^2)^2+(w_4*E_4*t_4^2)^2+2*w_3*w_4*E_3*E_4*t_3*t_4*(2*t
_3^2+3*t_3*t_4+2*t_4^2);
r=r2/r1;

theta1=l_p/r;
theta=theta1*180/pi;

%Deflection m
disp=r-r*cos(theta);
disp1=disp+l_t*sin(theta);
disp_M=[];
for i=1:1:5
    r1=6*t_3*t_4*E_3*E_4*t_3*t_4*(t_3+t_4)*(a_4-a_3)*delT_M(i);
```

```
r2=(w_3*E_3*t_3^2)^2+(w_4*E_4*t_4^2)^2+2*w_3*w_4*E_3*E_4*t_3*t_4*(2*t
_3^2+3*t_3*t_4+2*t_4^2);
    r=r2/r1;
    theta1=l_p/r;
    theta=theta1*180/pi;
    disp=r-r*cos(theta);
    disp_M=[disp_M disp+l_t*sin(theta)];
end
disp_Ex=xlsread('E:\Arslan Thesis\Design\Layout\Material
Properties.xlsx','Results_1','K100..O100');

figure(8)
    %subplot(4,3,8);
    plot(V_array,disp_M,'ro',V_array,disp_Ex,'ks');
    hold on;
    grid on;
    xlabel('Voltage (V)');
    ylabel('Displacement (um)');
    title('Displacement Vs Applied Voltage');

legend('Mathematical','Simulation','Location','northwest','Orientatio
n','horizontal');
    col_header={' ','Displacement'};
    xlswrite('E:\Arslan
Thesis\Matlab\data.xlsx',col_header,'Displacement','A1');
    col_header={'Voltage','Mathematical','Simulation'};
    xlswrite('E:\Arslan
Thesis\Matlab\data.xlsx',col_header,'Displacement','A2');
    xlswrite('E:\Arslan
Thesis\Matlab\data.xlsx',[V_array(:),disp_M(:),disp_Ex(:)],'Displacem
ent','A3');

%% Thermal Force
F_t=ky*disp1;
F_t_M=ky*disp_M;
F_t_Ex=ky*disp_Ex;
figure(9)
    %subplot(4,3,9);
    plot(V_array,F_t_M,'ro',V_array,F_t_Ex,'ks');
    hold on;
    grid on;
    xlabel('Applied Voltage');
    ylabel('Force (Micro Newtons)');
    title('Input Voltage Vs Force');

legend('Mathematical','Simulation','Location','northwest','Orientatio
n','horizontal');
    col_header={' ','Force'};
    xlswrite('E:\Arslan
Thesis\Matlab\data.xlsx',col_header,'Force','A1');
    col_header={'Voltage','Mathematical','Simulation'};
    xlswrite('E:\Arslan
Thesis\Matlab\data.xlsx',col_header,'Force','A2');
    xlswrite('E:\Arslan
Thesis\Matlab\data.xlsx',[V_array(:),F_t_M(:),F_t_Ex(:)],'Force','A3'
);
```

MATLAB CODE for Maximum Amplitude Vs Driving Frequency:

```
%% Maximum Amplitude Vs Driving Frequency
clear all
close all
clc

%%Input Parameter
V=1;                          %Voltage
V_array=[1 2 3 4 5];          %Voltage array

%% Dimensions of Actuator
%Thickness      m
t_1=1e-6;                     %Thickness of Silicon
t_2=0.3e-6;                   %Thickness of Silicon dioxide
t_3=0.3e-6;                   %Thickness of Poly Silicon
t_4=0.624e-6;                 %Thickness of Aluminum
t_5=20e-6;                    %Thickness of Tungsten
t_b=t_2+t_3+t_4;              %Beam Thickness

%Width of Beams m
w_1=0e-6;                     %Width of Silicon Beam
w_2=40e-6;                    %Width of Silicon Dioxide Beam
w_3=40e-6;                    %Width of Polysilicon Beam
w_4=40e-6;                    %Width of Aluminum Beam
w_5=10e-6;                    %Width of Tungsten Beam

%Length of Beams    m
l_1=0e-6;                     %Length of Silicon Beam
l_2=200e-6;                   %Length of Silicon Dioxide Beam
l_3=200e-6;                   %Length of Polysilicon Beam
l_4=200e-6;                   %Length of Aluminum Beam
l_5=1.074e-6;                 %Length of Tungsten Beam
l_r=l_3+l_4+.3e-6;            %Length of total resistive beam

%Proof mass Profile
l_p=700e-6;                   %Length of Proof mass
w_p=700e-6;                   %Width of proof mass
t_p=1.224e-6;                 %Thickness of proof mass
l_t=900e-6;                   %Length of Beam with Proof mass m

%Area of resistor m^2
A_r=t_3*w_3;                  %Area of resistor

%Volume of Used materials m^3
V_2=t_2*(l_2*w_2-t_5*w_5);    %Volume of SiO2 in Beam
V_3=t_3/2*(l_3*w_3-t_5*w_5)+t_3/2*(l_3*w_3);
%Volume of Polysilicon in Beam
V_4=t_4*(l_4*w_4-t_5*w_5);    %Volume of Aluminum in Beam
V_5=t_5*l_5*w_5;              %Volume of Tungsten in Beam
V_p=(l_p*t_p*w_p);            %Volume of SiO2 in Proof mass

%% Material Properties
%Thermal Conductivity W/m.K
tcon_1=157;                   %Thermal cond of Silicon
tcon_2=150;                   %Thermal cond of Silicon dioxide
tcon_3=200;                   %Thermal cond of Poly Silicon
tcon_4=236;                   %Thermal cond of Aluminum
tcon_5=187;                   %Thermal cond of Tungsten
```

```
tcon_avg=(tcon_2+tcon_3+tcon_4+tcon_5)/4;

%Densities      kg/m^3
pd_1=2328;                    %Density of Silicon
pd_2=2270;                    %Density of Silicon dioxide
pd_3=2300;                    %Density of Poly Silicon
pd_4=2700;                    %Density of Aluminum
pd_5=19250;                   %Density of Tungsten
pd_avg=(pd_2+pd_3+pd_4+pd_5)/4; %average density

%Young's Modulus    Pa
E_1=190e9;                    %Young's Modulus of Silicon
E_2=160e9;                    %Young's Modulus of Silicon dioxide
E_3=169e9;                    %Young's Modulus of Poly Silicon
E_4=70e9;                     %Young's Modulus of Aluminum
E_5=410e9;                    %Young's Modulus of Tungsten
E_avg=(E_2+E_3+E_4+E_5)/4;    %Average young's Modulus

%Co-efficient of thermal expansion 1/K
a_1=32e-7;                    %CTE Ratio of Silicon
a_2=29e-7;                    %CTE Ratio of Silicon dioxide
a_3=29.05e-7;                 %CTE Ratio of Poly Silicon
a_4=230e-7;                   %CTE Ratio of Aluminum
a_5=45e-7;                    %CTE Ratio of Tungsten

%Resistivity    ohm.m
p_1=0.023;                    %Resistivity of Silicon
p_2=1.1e15;                   %Resistivity of Silicon dioxide
p_3=9.2e-6;                   %Resistivity of Poly Silicon
p_4=2.71e-8;                  %Resistivity of Aluminum
p_5=5.6e-8;                   %Resistivity of Tungsten
p_avg=(p_3+p_4)/2;            %Average resistivity of conducting beam

%Mass of single beam kg
m_1=(w_1*t_1*l_1)*pd_1;       %Mass of Silicon in a Beam
m_2=(w_2*t_2*l_2)*pd_2;       %Mass of Silicon dioxide in a Beam
m_3=(w_3*t_3*l_3)*pd_3;       %Mass of Polysilicon in a Beam
m_4=(w_4*t_4*l_4)*pd_4;       %Mass of Aluminum in a Beam
m_5=(w_5*t_5*l_5)*pd_5;       %Mass of Tungsten in a Beam
m_p=(l_p*t_p*w_p)*pd_2;       %Mass of Proof mass
M=m_2+m_3+m_4+m_5+m_p;        %Mass of Beam with Proof mass

%% Spring Constant or Stiffness N.m
N=4;                          %Total numbers of beams
ky=(((E_4*w_4*(t_b)^3)/(l_4)^3)/4)/N;
                              %Spring constant
%% Effective Mass kg
M_2=pd_2*V_2;                 %Mass of SiO2 in Beam
M_A=pd_2*(1.5568e-13);        %Mass of SiO2 in Anchor
M_p=pd_2*V_p;                 %Mass of SiO2 in Proof mass
M_3=pd_3*V_3;                 %Mass of Polysilicon in Beam
M_4=pd_4*V_4;                 %Mass of Aluminum in Beam
M_5=pd_5*V_5;                 %Mass of Tungsten in Beam
M=pd_avg*(200e-6*40e-6*1.224e-6)+m_p;
                              %Average mass of wing

%% Resonance Frequency Hz
wn=sqrt(ky/M);                %Angular Resonance frequency

%% Damping
```

```
g_o=50e-6;              %Distance b/w cantilever and the substrate
u_a=1.81e-15;           %Viscosity of air
n_al=17.59e-6;          %Damping coefficient of aluminum (17.59kg/s)
pd_air=1.225;           %Density of Air in kg/m^3

%Air Flow Damping
D_air=(3*pi*(u_a)*(w_3))+((3/4)*pi*(w_3)^2*sqrt(2*u_a*pd_air*wn));

%Structural Damping
D_struc=(n_al/wn)*ky;

%Squeeze Film Damping
D_sque=(u_a)*(w_3)/(2*(pd_avg)*(g_o)^3*(t_b)*wn);

%Anchor Loss Damping
D_anchor=(0.23*(t_b)^3)/(l_3)^3;

%Total Damping
b=D_air+D_struc+D_sque+D_anchor;    %Damping
gema=b/M;                           %Damping Constant
zeta=gema/(2*wn);                   %Zeta

%Quality Factor
Q=(wn)/gema;                        %Quality Factor


%% Changings in Electro-thermal actuator
%Thermal resistance K/W
Rth_2=(1/tcon_2)*(t_2/(w_2*l_2));
Rth_3=(1/tcon_3)*(t_3/(w_3*l_3));
Rth_4=(1/tcon_4)*(l_4/(w_4*t_4));
Rth=Rth_2+Rth_3+Rth_4;

%Current        A
I=((1/p_avg)*V*A_r/l_r);            %Current A

I_M=[];
for i=1:1:5
    I_M=[I_M ((1/p_avg)*V_array(i)*A_r/l_r)];
end

%Change in Temperature  K
delT=(I^2*Rth)/(l_3*tcon_3);
delT_M=[];
for i=1:1:5
delT_M=[delT_M (I_M(i)^2*Rth)/(l_3*tcon_3)];
end

%Radius of curvature of arc m
r1=6*t_3*t_4*E_3*E_4*t_3*t_4*(t_3+t_4)*(a_4-a_3)*delT;
r2=(w_3*E_3*t_3^2)^2+(w_4*E_4*t_4^2)^2+2*w_3*w_4*E_3*E_4*t_3*t_4*(2*t
_3^2+3*t_3*t_4+2*t_4^2);
r=r2/r1;

theta1=l_p/r;                       %Theta in radians
theta=theta1*180/pi;                %%Theta in degrees

%Deflection m
```

```
disp=r-r*cos(theta);
disp1=disp+l_t*sin(theta);
disp_M=[];
for i=1:1:5
    r1=6*t_3*t_4*E_3*E_4*t_3*t_4*(t_3+t_4)*(a_4-a_3)*delT_M(i);

r2=(w_3*E_3*t_3^2)^2+(w_4*E_4*t_4^2)^2+2*w_3*w_4*E_3*E_4*t_3*t_4*(2*t
_3^2+3*t_3*t_4+2*t_4^2);
    r=r2/r1;
    theta1=l_p/r;
    theta=theta1*180/pi;
    disp=r-r*cos(theta);
    disp_M=[disp_M disp+l_t*sin(theta)];
end
disp_Ex=xlsread('E:\Arslan Thesis\Design\Layout\Material
Properties.xlsx','Results_1','K100..O100');

%% Thermal Force
F_t=ky*disp1;
F_t_M=ky*disp_M;
F_t_Ex=ky*disp_Ex;
FT_M=zeros(1,10);
fr_Ex=976;      %frequency of 1st mode in intellisuite
wn_Ex=fr_Ex*2*pi;
for x=5:5;
    FT_M=0;
    FT_Ex=0;
    FT_M=F_t_M(x);
    FT_Ex=F_t_Ex(x);
    A_M=[];
    A_Ex=[];
    f=[];

%% Amplitude at Resonance Frequency
for wd=100:100:10000;                        %Angular Driving Frequency
    f=[f (wd)/(2*pi)];                       %Driving frequency
    A_M=[A_M ((((FT_M)/M)/(sqrt(((wn^2-
wd^2)^2)+(wd.*gema)^2)))./10^(-6))];
    A_Ex=[A_Ex ((((FT_Ex)/M)/(sqrt(((wn_Ex^2-
wd^2)^2)+(wd.*gema)^2)))./10^(-6))];         %FT_Ex Simulated force
end

fd=f;             % Array of Driving frequency
figure(10)
    %subplot(4,3,10);
    plot(fd,A_M,'--ro',fd,A_Ex,'--ks');
    hold on;
    grid on;
    xlabel('Driving Frequency');
    ylabel('Amplitude (Micrometers)');
    title('Amplitude Vs Frequency');

legend('Mathematical','Simulation','Location','northwest','Orientatio
n','horizontal');
    col_header={' ','Amplitude'};
    xlswrite('E:\Arslan
Thesis\Matlab\data.xlsx',col_header,'Amplitude','A1');
    col_header={'Frequency','Mathematical','Simulation'};
    xlswrite('E:\Arslan
Thesis\Matlab\data.xlsx',col_header,'Amplitude','A2');
```

```
    xlswrite('E:\Arslan
Thesis\Matlab\data.xlsx',[fd(:),A_M(:),A_Ex(:)],'Amplitude','A3');

end
```

References

[1] E. Mastropaolo, G. S. Wood, I. Gual, P. Parmiter, and R. Cheung, "Electrothermally actuated silicon carbide tunable MEMS resonators," *J. Microelectromechanical Syst.*, vol. 21, no. 4, pp. 811–821, 2012.

[2] A. Jafarpour and H. B. Ghavifekr, "A Novel MEMS Enabled JElectro-thermally Actuated Frequency Tunable Micrstrip Patch Antenna," *25th Iran. Conf. Electr. Eng. (lCEE20 17)*, pp. 426–430, 2017.

[3] P. J. Gilgunn, J. Liu, N. Sarkar, and G. K. Fedder, "CMOS-MEMS lateral electrothermal actuators," *J. Microelectromechanical Syst.*, vol. 17, no. 1, pp. 103–114, 2008.

[4] Y. Y. Feng, S. J. Chen, and P. H. Hsieh, "Fabrication of an Electro-Thermal Micro Gripper Using Silver-Nickel Ink," *Proc. IEEE Int. Conf. Micro Electro Mech. Syst.*, no. J24–28 January 2016, pp. 1141–1144, 2016.

[5] D. S. Chen *et al.*, "An Electrothermal actuator with two degrees of freedom serving as the arm of a MEMS gripper," *IEEE Trans. Ind. Electron.*, vol. 61, no. 10, pp. 5465–5471, 2014.

[6] W. Wang, Q. Chen, D. Wang, L. Zhou, and H. Xie, "A bi-directional large-stroke electrothermal MEMS mirror with minimal thermal and temporal drift," *Proc. IEEE Int. Conf. Micro Electro Mech. Syst.*, no. 22-26 January, 2017, pp. 331–334, 2017.

[7] T. Dhakshina Moorthy and P. Nair, "Modeling 3-dimensional electro thermal actuation of MEMS mirrors," *2017 Int. Conf. Nextgen Electron. Technol. Silicon to Software, ICNETS2 2017*, no. 4, pp. 117–121, 2017.

[8] E. Bertarelli, A. Colnago, R. Ardito, G. Dubini, and A. Corigliano, "Modelling and characterization of circular microplate electrostatic actuators for micropump applications," *2015 16th Int. Conf. Therm. Mech. Multi-Physics Simul. Exp. Microelectron. Microsystems,* pp. 1–7, 2015.

[9] E. Brusa, G. De Pasquale, and A. Somà, "Experimental characterization of electro-thermo-mechanical coupling in gold RF microswitches," *J. Microelectromechanical Syst.*, vol. 22, no. 4 August,2013, pp. 919–929, 2013.

[10] J. Varona, M. Tecpoyotl-Torres, J. Escobedo-Alatorre, and A. A. Hamoui, "Design and fabrication of a MEMS thermal actuator for 3D optical switching applications," *LEOS Summer Top. Meet.*, pp. 31–32, 2008.

[11] R. C. Voicu, C. Tibeica, R. Muller, and A. Dinescu, "An SU-8 micro-tweezer based on the chevron electro-thermal actuators with a large in-plane displacement," *Proc. Int. Semicond. Conf. CAS*, vol. October, 2, pp. 105–108, 2017.

[12] X. Zhang, L. Liu, W. Liang, X. Li, and H. Xie, "An electrothermal/electrostatic dual driven MEMS scanner with large in-plane and out-of-plane displacement," *Int. Conf. Opt. MEMS Nanophotonics*, no. August, pp. 13–14, 2013.

[13] T. Moulton and G. K. Ananthasuresh, "Micromechanical devices with embedded electro-thermal-compliant actuation," *Sensors Actuators, A Phys.*, vol. 90, no. 1–2, pp. 38–48, 2001.

[14] M. H. Hristov, T. B. Takov, I. N. Cholakova, K. H. Denishev, V. E. Grozdanov, and D. G. Gaydazhiev, "DESIGN AND INVESTIGATION OF A THERMAL ACTUATOR," *ELECTRONICS*, no. 09-2008, pp. 43–48, 2008.

[15] K. S. Member *et al.*, "Hybrid Dynamic Modeling of V-Shaped Thermal Micro-Actuators," *2016 17th Int. Conf. Therm. Mech. Multi-Physics Simul. Exp. Microelectron. Microsystems*, pp. 5–8, 2016.

[16] Z. Zhang, Y. Yu, X. Liu, and X. Zhang, "Dynamic modelling and analysis of V- and Z-shaped electrothermal microactuators," *Microsyst. Technol.*, vol. 23, no. 8, pp. 3775–3789, 2017.

[17] C. Lee, "A MEMS VOA using electrothermal actuators," *J. Light. Technol.*, vol. 25, no. 2, pp. 490–498, 2007.

[18] S. Banerji, D. Fernandez, and J. Madrenas, "Characterization of CMOS-MEMS Resonant Pressure Sensors," *IEEE Sens. J.*, vol. 17, no. 15 October, 2017, pp. 6653–6661, 2017.

[19] J. Reinke, G. K. Fedder, and T. Mukherjee, “CMOS-MEMS variable capacitors using electrothermal actuation,” *J. Microelectromechanical Syst.*, vol. 19, no. 5, pp. 1105–1115, 2010.

[20] G. Skidmore *et al.*, “Parallel assembly of microsystems using Si micro electro mechanical systems,” *Microelectron. Eng.*, vol. 67–68, pp. 445–452, Jun. 2003.

[21] S. V. Estahbanati, M. Bakri-Kassem, and R. Dhaouadi, “Nonlinear modeling and characterization of a thermally driven MEMS actuator with a folded spring reference beam,” in *2017 18th International Conference on Thermal, Mechanical and Multi-Physics Simulation and Experiments in Microelectronics and Microsystems (EuroSimE)*, 2017, pp. 1–4.

[22] X. Li, Y. Zhao, and T. Hu, “Design Of A Novel Electrothermal Actuator for Integrated MEMS Safety-and-Arming Devices,” pp. 63–66, 2015.

[23] B. Piriyanont, S. O. R. Moheimani, and A. Bazaei, “Design and control of a MEMS micro-gripper with integrated electro-thermal force sensor,” *2013 IEEE/ASME Int. Conf. Adv. Intell. Mechatronics Wollongong, Aust.*, no. 9–12July,2013, pp. 479–484, 2013.

[24] D. Girbau, L. Pradell, A. Lázaro, and À. Nebot, “Electrothermally actuated RF MEMS switches suspended on a low-resistivity substrate,” *J. Microelectromechanical Syst.*, vol. 16, no. 5, pp. 1061–1070, 2007.

[25] M. Rakotondrabe, A. G. Fowler, and S. O. R. Moheimani, “Control of a novel 2-DoF MEMS nanopositioner with electrothermal actuation and sensing,” *IEEE Trans. Control Syst. Technol.*, vol. 22, no. 4, pp. 1486–1497, 2014.

[26] H. Wang, L. Zhou, X. Zhang, and H. Xie, “Thermal Reliability Study of an Electrothermal MEMS Mirror,” *IEEE Trans. Device Mater. Reliab.*, vol. PP, no. c, p. 1, 2018.

[27] D. O. Popa, Byoung Hun Kang, J. T. Wen, H. E. Stephanou, G. Skidmore, and A. Geisberger, “Dynamic modeling and input shaping of thermal bimorph MEMS actuators,” *2003 IEEE Int. Conf. Robot. Autom. (Cat. No.03CH37422)*, vol. 1, pp. 1470–1475, 2003.

[28] J. J. Khazaai and H. Qu, “Electro-thermal MEMS switch with latching

mechanism: Design and characterization," *IEEE Sens. J.*, vol. 12, no. 9, pp. 2830–2838, 2012.

[29] Z. Zhang, Y. Yu, X. Liu, and X. Zhang, "Dynamic electro-thermal modeling of V- and Z-shaped electrothermal microactuator," *2016 IEEE Int. Conf. Mechatronics Autom. IEEE ICMA 2016*, pp. 890–895, 2016.

[30] C. Lee, "A MEMS VOA Using Electrothermal Actuators," vol. 25, no. 2, pp. 490–498, 2007.

[31] Xing Yang, C. Grosjean, and Yu-Chong Tai, "Design, fabrication, and testing of micromachined silicone rubber membrane valves," *J. Microelectromechanical Syst.*, vol. 8, no. 4, pp. 393–402, 1999.

[32] H. Sumali and T. G. Carne, "Air-drag damping on micro-cantilever beams," *Conf. Proc. Soc. Exp. Mech. Ser.*, 2008.